NASA-TM-80170 19800002215

NASA Technical Memorandum 80170

AN EXPERIMENTAL INVESTIGATION TO DETERMINE THE EFFECT OF WINDOW COOLING BY MASS INJECTION FOR THE SHUTTLE INFRARED LEESIDE TEMPERATURE SENSING (SILTS) EXPERIMENT

Pamela F. Bradley

September 1979

National Aeronautics and
Space Administration

Langley Research Center
Hampton, Virginia 23665

AN EXPERIMENTAL INVESTIGATION TO DETERMINE THE EFFECT OF WINDOW COOLING BY MASS INJECTION FOR THE SHUTTLE INFRARED LEESIDE TEMPERATURE SENSING (SILTS) EXPERIMENT

Pamela F. Bradley
Langley Research Center

SUMMARY

An experimental test program was conducted in the Langley continuous flow hypersonic tunnel to determine the effect of mass injection on the Shuttle Infrared Leeside Temperature Sensing (SILTS) pod window surfaces in reducing window heating and minimizing window lens radiation during the reentry data-taking period. Because high window temperatures will affect the infrared radiation received by the SILTS sensor during reentry, mass injection at the base of the window lenses is used as a means of maintaining low window temperatures. A 0.25-scale model of a portion of the orbiter's vertical tail with a SILTS pod was fabricated of stainless steel and instrumented with thermocouples in order to determine heat-transfer coefficients on and around the simulated windows and window cavities. Wind-tunnel tests were conducted over a Reynolds number range of 1.64×10^6 to 7.22×10^6 per meter at corresponding free-stream Mach numbers of 10.16 to 10.36.

Two window-cavity configurations were tested. Results indicate that deeper window cavities provide more thermal protection for the window surfaces, especially when there is no coolant flow. A coolant mass flow, the order of the local free stream ahead of the orbiter's vertical tail, will reduce heating to the window surfaces by 90 percent.

INTRODUCTION

The Space Shuttle Orbiter will provide scientists and engineers an opportunity to conduct flight experiments in the hypersonic environment. The Shuttle Infrared Leeside Temperature Sensing (SILTS) experiment is one of several experiment packages within the Orbiter Experiments Program (OEX) (ref. 1), presently being designed to obtain flight data (refs. 2 and 3). An infrared scanner will be mounted inside a cylindrical protective pod on the tip of the orbiter's vertical tail. The scanner will view the upper surfaces of the fuselage and wing (fig. 1) through two windows which are recessed into the cylinder's hemispherical nose cap. Data from the scanner will be recorded on an onboard recorder. Leeside surface temperatures determined from these data will provide the basis for calculating heating distributions over the upper surfaces.

Accuracy of leeside temperatures will be degraded if the transparent window material through which the scanner views the leeside also emits significant radiation. As the window temperature increases, the window emits more radiation and also loses transmission. For this reason, the window-material temperatures must remain low during the reentry data period. Predicted design heating rates in the vicinity of the SILTS pod result in radiation equilibrium surface temperatures of the order of 1500K. If window temperatures are also allowed to reach such high temperatures, the transmitted infrared will be altered; therefore, cooling of the windows is necessary.

Experimental or analytical data for aerodynamic heating in and around cavities with or without a cooling fluid injected into the bottom of the cavity are not generally available in the literature. Furthermore, the stream conditions ahead of the pod and cavities were not clearly defined at the time of this investigation. The orbiter enters the atmosphere at an angle of attack of as much as 40^{o}, and the pod in its location at the tip of the vertical tail is submerged in fuselage wake flow. The conceptual plan for cooling the SILTS windows consisted of injecting a cooling gas, which is to be stored onboard the orbiter, into the bottom of the cavities. In order to simplify the cooling system, it was elected to supply an approximately constant cooling flow rate to the windows. Under this system, the initial entry into the rarefied upper atmosphere would have massive cooling flow rates (compared to the free-stream mass flow). As the reentry progresses into the more dense portions of the atmosphere, the cooling mass injected becomes less in comparison to the stream mass flow. Thus the question of window cooling becomes one of determining the altitude or mass-flow ratio (coolant to stream mass flow) at which the onset of window heating occurs.

The present investigation was undertaken to determine experimentally the effects of cooling by mass injection on the window surfaces of a SILTS pod. Tests were conducted in the Mach 10 continuous flow hypersonic tunnel on a 0.25-scale model of a portion of the orbiter's modified vertical tail and the hemispherically domed pod which will hold the SILTS camera. Wind-tunnel tests were conducted over a Reynolds number range of 1.64×10^{6} to 7.22×10^{6} per meter at corresponding free-stream Mach number of 10.16 to 10.36. Room-temperature air was injected into each of the two window cavities from holes at the base of each window. The mass-flow-rate range tested was from zero to 0.004 kg/sec. Heat-transfer rates were measured on and around simulated windows and window cavities on the model. Also, oil-flow photographs were used to interpret the flow fields producing the heating.

Since the entire orbiter is not being tested in this investigation, the free-stream conditions in this test are those directly ahead of the model of the SILTS pod. Use of these results in flight requires that the ratio of the local stream condition which could exist ahead of the SILTS pod to the free-stream conditions ahead of the orbiter be known for the appropriate vehicle attitude and flight conditions.

SYMBOLS

A	area, m^2
$a,b,c,$	constants for equations (2) and (3)
c_p	specific heat, j/kg-K
d	hemisphere diameter, cm
h	heat-transfer coefficient, W/m^2-K
M	Mach number
$\dot{m}$	mass-flow rate, kg/sec

p	pressure, Pa
q	heating rate, W/m^2
R	gas constant, m^2/sec^2-K
r	recovery factor
s_1	model body coordinate, cm
T	temperature, K
t	time, sec
x_1, x_2	model horizontal coordinate
α	coordinate on window surfaces and in cavities, degrees
γ	ratio of specific heats
λ	local model skin thickness, cm
ρ	density, kg/m^3

Subscripts

2	conditions behind the shock
aw	adiabatic wall
c	coolant
L	local flow conditions
m	model
o	stagnation-point conditions
t	total
w	wall
∞	free-stream conditions

APPARATUS AND PROCEDURE

Facility

The investigation was conducted in the Langley Research Center continuous flow hypersonic tunnel which is a nominal Mach 10 air facility. A description of the facility and its capabilities may be found in references 4 and 5. For this test, the free-stream Reynolds number range was 1.64×10^6 to 7.22×10^6 per meter with an average air-stagnation temperature of 1000K. Because the Mach 10 flow deviates slightly from a perfect gas, real-gas corrections for the perfect-gas relations of reference 6 were deduced using the method of Erickson and Creekmore (ref. 7).

Models and Instrumentation

The 0.25-scale model of the SILTS configuration was fabricated of 347 stainless steel sheet. Figure 2 shows the portion of the orbiter's vertical tail which the model represented. Figures 3 and 4 are photographs of the model in the tunnel. General model dimensions and thermocouple array names are shown in figure 5. The model is mounted to the injection plate such that the model's leading edge is horizontal in the tunnel (as shown in fig. 3); the +x direction is the flow direction in the tunnel. The location of $x_1 = 0$ and $s_1 = 0$ is at the stagnation point of the model hemisphere. The location of $x_2 = 0$ is on the leading edge of the fin portion of the model. Thermocouple locations that are nondimensionalized by the hemisphere's diameter and peripheral locations (α) of thermocouples on the windows and in window cavities are listed in table I. Schematic thermocouple locations for the two window-configuration cavities and surfaces are given in figure 6. Closeups of the nose-cap window Configurations I and II are shown in figures 7 and 8. Details of the two window configurations are shown in figure 9. Configuration I was instrumented with 62 chromel-alumel thermocouples and Configuration II was instrumented with 34 thermocouples located only in the two window cavities.

Window 1 of Configurations I and II is located on the centerline of the hemisphere 37° below the stagnation point. Window 2 of Configuration I is located 66° below and 42° to the right of the stagnation point; window 2 of Configuration II is located 55° below and 50° to the left of the stagnation point. Window 2 of Configurations I and II is not at the same location as a result of design changes which took place between construction of the two model configurations. In the final configuration, window 2 will be located to the right (fig. 7) of the centerline. As a result of the different locations for window 2, direct comparisons of the data cannot be made.

Each window has four 0.264-cm diameter orifices through which coolant air was blown (see fig. 9). The instrumented window surfaces were insulated on the back side to insure that the window cooling effect measured represented the blocking effect of the coolant on the window exterior and not convective cooling of the window interior surface. No interior-surface cooling will be provided in the flight configuration.

L. F

t air was drawn from the tunnel's service air line.
varied the line pressure to a mass-flow panel over
4×10^5 Pa. The regulating unit can provide mass
to full-scale reading over four ranges (0.0045,
). A range of coolant mass flows was obtained by
line to the panel.

Test Procedures

the surface of the SILTS configuration model were
-calorimeter technique (ref. 8). Prior to test
olated from the tunnel in the injection box. Once
del was injected for a test sequence. After data
retracted, and air jets were used to cool the
preparation for the next test. For tests with
ne desired window-coolant flow rate ($\dot{m}_c$* in the
initiated prior to injection into the tunnel. Large
eased the injection-box pressure sufficiently to
the sidewall door was opened. A delaying circuit
between the door seal being deflated and the door
the air mass in the injection box to be slowly
vented into the test section. A matrix of test conditions is given in table II.

Oil-flow tests to determine the surface flow producing the heating characteristics were conducted in a similar manner. The model was coated with clear silicone oil and splattered with oil mixed with lamp black. The model was injected into the hypersonic stream for 10 seconds and then retracted into the injection box. The injection box was then rotated to the service position and photographs were taken of the model.

Data Reduction

Rapid injection of the SILTS model provided approximately a step-input temperature to the model. Heat-transfer rates were determined using the thin-skin approximation with

$$q = \rho_m C_{p,m} \lambda \frac{\partial T_w(t)}{\partial t} \tag{1}$$

$\partial T_w/\partial t$ was calculated from the data, after the initial transient passed. Basically, by curve-fitting the data, wall temperature was represented as a quadratic function of time (eq. (2)) such that

$$T_w = a + bt + ct^2 \tag{2}$$

---

*$\dot{m}_c$ is the total coolant flow which was equally divided between the two windows.

and

$$\frac{\partial T_w}{\partial t} = b + 2ct \tag{3}$$

where a, b, and c were the computed constants of the curve fit.

Then, heat-transfer coefficient was calculated using the following equation.

$$h = \frac{q}{T_t - T_w} \tag{4}$$

Total temperature, T_t, was used instead of T_{aw} in equation (4) for this investigation because of a lack of knowledge of the correct values for T_{aw}. The range of possible errors in heat-transfer coefficient resulting from this assumption is estimated to be from zero at the stagnation point to 13 percent. The ratio of coolant to free-stream mass flow was calculated for two windows using:

$$\dot{m}_c/\dot{m}_\infty = (\dot{m}_{coolant})_{measured} \Big/ \left(2A_{window}\ P_\infty\ M_\infty \sqrt{\gamma/RT}\right) \tag{5}$$

RESULTS AND DISCUSSION

Oil Flow

The model's flow field is complicated by the interaction of flows over a blunted wedge and a hemisphere with surface cavities. A general description of the surface flow field can be determined from the oil-flow photographs of Configuration I shown in figures 10 through 14.

Figures 10 and 11 illustrate the hemisphere-surface flow pattern modified by the addition of window cavities. At the entrance to the window 1 cavity, the flow separates and then reattaches on the downstream cavity walls. With mass injection, as shown in figure 11, the separation line moves up the cavity wall closer to the hemisphere stagnation point. The oil pattern is much lighter at the bottom of the window 1 cavity, indicating a higher surface shear than surrounding areas. This flow merges with that coming from the hemisphere stagnation point, forming an oil-accumulation line on the hemisphere.

With no mass injection as shown in figure 12, the surface flow on the side of the hemisphere is deflected up away from the window 2. A comparison of figures 12 (no mass injection) and 13 (mass injection view of the side of the model with window 2) shows the effect mass injection has on the feather pattern just below window 2. The feather pattern, which generally indicates the existence of vortical flow field, is somewhat compressed below window 2, showing that the coolant flow has perturbed the flow field. Even with mass injection, as in figure 14, there is no deflection of the surface flow on the side of the hemisphere with no window.

Figure 15 shows Configuration II with the flow deflected up away from window 2, even though window 2 is farther away from hemipshere-fin intersection.

Heat Transfer

Heat-transfer results are presented only for a Reynolds number of 1.64×10^6 per meter since the results for the higher Reynolds numbers were similar to those obtained for the low Reynolds numbers. Figures 16 through 21 present the data in terms of h/h_o for coolant-mass-flow-rate ratios $(\dot{m}_c/\dot{m}_\infty)$ from zero to 2.9. h_o is a reference stagnation-point, heat-transfer coefficient for a 0.3048-m radius sphere scaled from the full-scale orbiter to the 0.25-scale model of this test.

The ratio of local stagnation-point, heat-transfer coefficient ahead of the pod on the complete orbiter configuration to an orbiter-nose, stagnation-point coefficient was determined from a total pressure measurement in the vicinity of the pod with an approximation of Fay and Riddell's (ref. 9) stagnation-point, heat-transfer-coefficient equation.

$$\frac{h_{o,POD}}{h_{o,NOSE}} = \sqrt{\frac{P_{t,2,POD}}{P_{t,2,NOSE}}} \tag{6}$$

The value selected from a number of different test conditions was $h_{o,POD}/h_{o,NOSE} = 0.216$. These results are unpublished. Thus the quantity h/h_o, as plotted in figures 16 through 21, represents the ratio of the measured heating to a reference sphere heating rate in the free stream ahead of a complete orbiter configuration. In this form, the results may be conveniently used in flight calculations. Scaling for this test was accomplished by specifications established for the SILTS experiment program.

Zero mass injection (Configuration I).- Distributions of heating on the vertical plane of symmetry for zero mass injection are shown in figure 16 (data represented by circle symbols). The data are plotted from the top of the hemisphere, around the contour of the hemisphere, through window 1, and along the model's fin leading edge. The heat-transfer coefficient increases from its value at the top of the hemisphere to its stagnation-point location at $s_1 = 0$. Without mass injection, heating on window 1 is 20 to 40 percent higher than the stagnation point value. Just below the hemisphere-fin intersection, the heating is almost three times that at the stagnation point as a result of the bow-shock-fin shock interaction and the deviation from perfect hemisphere flow. Along the fin's leading edge, heating gradually decreases to the stagnation-point value as the influences of the hemisphere-fin intersection region become less.

Figure 17 shows that the fin chordwise heating drops to less than 10 percent of stagnation heating two diameters downstream of the fin leading edge. Near $x_2/d = 0.75$, the heating rises to 70 percent of the leading-edge

value. This is the result of shear-layer impingement from the shock-interaction region.

Figures 18 and 19 show distributions of heating on the two window surfaces. Because they are not part of the ring of surface thermocouples located on a 1.11-cm diameter from the center of the window surfaces, the center thermocouples are plotted at $\alpha = 0^{\circ}$, but are not included as part of the faired curve. Heating is fairly constant over the window 1 surface and, as mentioned previously, is higher than the hemisphere-stagnation-point heating. The window 2 surface, located close to the hemisphere-fin intersection, experiences heating 75-percent higher than that at the hemisphere stagnation point.

Farther out along the window fairings (Configuration I) is the outer ring of thermocouples (figs. 20 and 21). Close to the fin, the heating on the window 1 fairing increases to a value twice that of the hemisphere stagnation heating. However, the attached flow heating remains very close to the stagnation value at the entrance to the cavity below the stagnation point. In figure 21, the heat-transfer coefficient ratio remains fairly constant at 0.15 for α less than 200°, but has a peak in heating on the downstream side of the fairing.

Mass injection (Configuration I).- Mass injection provides large reductions in heating from zero-mass-injection levels for the window and surrounding surfaces. On the fin leading edge (fig. 16), the highest heating peak near the hemisphere-fin intersection is reduced significantly by mass injection. Heating on the window 1 surface is reduced more than 90 percent for injection-mass-flow ratios of less than one, and heating to the surrounding areas is generally reduced by 60 percent. In figure 17, coolant injection from window 2 is seen to reduce heating up to 40 percent on the fin in the shear-layer region. (For Configuration I, window 2 is below window 1 and very close to the fin). As shown in figure 19, for injection ratios above 0.35, heat transfer is reduced from its highest value, 0.35, to less than 0.01 over the entire window surface. This reduction in surface heating is shown further in figure 22 (window 1) and figure 23 (window 2) as a function of injection ratio for each window's center thermocouple.

The outer-ring data for window 1 and 2 are presented in figures 20 and 21, respectively. Heating on window 1 is reduced by an average of 60 percent. Increases in coolant injection for this window produced an irregular flow field and, consequently, data scatter. With injection, heating to window 2 (fig. 21) is reduced by 80 to 90 percent--including the peak in heating mentioned for zero mass injection.

Comparison of data from the two window geometries.- The Configuration II window geometry with sharp-cornered edges was tested for comparison with the Configuration I window geometry. The two geometries are shown in figure 9. A comparison between the two window geometries shows that mass injection provides similar reductions in heating to the window surfaces for both configurations. The data that will be presented here is, therefore, a comparison between the two geometries with zero mass injection. Because the location of window 2 was changed in addition to the changes in window-cavity depth, comparisons between

Configuration I and II would not lead to distinquishing between cavity-depth effects and window-location effects. Therefore, only a comparison of data from window 1 of both configurations will be presented and will give an indication of cavity-depth effects.

On the window 1 surface (fig. 24), the Configuration II heat-transfer coefficients are up to 30-percent lower than those of Configuration I. Also for Configuration II, a ring of thermocouples gives heat-transfer data at the location in the cavity where the diameter of the cavity is 1.8 cm., or approximately halfway from the window surface to the lip. This set of data is compared with the outer-ring data from Configuration I, since the outer ring from Configuration I is located at the same diameter. As shown in figure 25, reductions in heating of up to 60 percent are noted with the deeper cavity. The dip in heating for Configuration II in the vicinity of $\alpha = 90^\circ$ and $\alpha = 270^\circ$ suggests a region of flow intersection between the flow coming down the hemisphere from the stagnation point and up from the fin into the window 1 cavity, as in Configuration I.

Figure 26 shows the heating for the two Configuration II windows at the outer-ring station where the hemisphere and cavity intersect. Because it is close to the high heating of the stagnation region, the window 1 heating is up to 35-percent higher than window 2. The highest heating on window 1 is near the fin-pod junction, around $\alpha = 200^\circ$, where shock interaction is the major heating factor. From figures 20 and 21, the Configuration I outer-ring data indicate that the heating on the fairing of the Configuration I windows is influenced by the fin-pod intersection--a region of high heating in relatively stagnant flow. The outer-ring data of Configurations I and II and oil-flow photographs verify that this is a region of high heating. The outer-ring data of Configuration II for window 2 generally follow the trends from the middle ring, with the highest heating near $\alpha = 180^\circ$, closest to the fin.

CONCLUSIONS

An experimental investigation was conducted to determine the effects of mass injection on the SILTS window surfaces during orbiter reentry. This test program was performed in the Langley Research Center continuous flow hypersonic tunnel over a range of free-stream Reynolds numbers from 1.64×10^6 to 7.22×10^6 per meter. The test results for one Reynolds number were presented as a representative sample of the data in the form of heat-transfer coefficients normalized to a stagnation-point, heat-transfer coefficient for a scaled 0.3048-m radius sphere in the free stream ahead of a complete orbiter configuration. Comparisons of data from two different window-cavity geometries were documented.

Conclusions drawn from the results are:

1. Oil-flow photographs and reductions in heating indicate that mass injection affects the flow field near the SILTS windows--especially on the leading edge of the fin.

2. Coolant-flow-rate ratios of the order of one reduce heating on the window surfaces by 90 percent.

3. The deeper cavity windows (Configuration II) provide reductions in heating similar to those determined for Configuration I with mass injection. The Configuration II geometry also reduces heating on the window 1 surface, when there is no mass injection, by 30 percent.

4. In Configuration II, the sharp-edged corner junction between the window cavities and the hemisphere causes no large increase in heating, over the fairing of Configuration I.

REFERENCES

1. Siemers, P. M., III; and Larson, T. J.: The Space Shuttle Orbiter and Aerodynamic Testing. AIAA Paper No. 78-790. Presented at the AIAA 10th Aerodynamic Testing Conference, April 1978.

2. Siemers, P. M., III: Shuttle Entry Technology Payloads. AIAA Paper No. 75-251. Presented at the AIAA 21st Annual Meeting of the American Astronautical Society--"Space Shuttle Missions of the 80's," August 1975.

3. Dunavant, J. C.; Narayan, K. Y.; and Walberg, G. D.: A Survey of Leeside Flow and Heat Transfer on Delta Planform Configurations. AIAA Paper No. 76-118. Presented at the AIAA 14th Aerospace Sciences Meeting, January 1976.

4. Schaefer, W. T., Jr.: Characteristics of Major Active Wind Tunnels at the Langley Research Center. NASA TM—1130, July 1965.

5. Pirrello, C. J.; Hardin, R. D.; Heckart, M. V.; and Brown, K. R.: An Inventory of Aeronautical Ground Research Facilities, Vol. I - Wind Tunnels. NASA CR-1874, November 1971.

6. Ames Research Staff: Equations, Tables and Charts for Compressible Flow. NASA TR-1135, 1953.

7. Erickson, Wayne D.; and Creekmore, Helen S.: A Study of Equilibrium Real-Gas Effects in Hypersonic Air Nozzles, Including Charts of Thermodynamic Properties for Equilibrium Air. NASA TN D-231, April 1960.

8. Dunavant, J. C.; and Stone, H. W.: Effect of Roughness on Heat Transfer to Hemisphere Cylinders at Mach Numbers of 10.4 and 11.4. NASA TN D-3871, March 1967.

9. Fay, J. A.; and Riddell, F. R.: Theory of Stagnation Point Heat Transfer in Dissociated Air. Journal of the Aeronautical Sciences, Vol. 25, No. 2, February, 1958, pp. 73-85.

TABLE 1.- THERMOCOUPLE LOCATIONS FOR CONFIGURATIONS I AND II

CONFIGURATION I

Thermocouple	x_1/d	x_2/d	s_1/d	α (°)
1	-	-	0.1309	-
2	0.0	0.0	0.0	-
3	0.1309	-	-	-
4	0.2618			
5	0.3927	-	-	-
6	0.5236	-	-	-
7	0.6545	-	-	-
8	-	-	-0.1309	-
9	-	-	-0.2618	-
10	-	-	-0.3927	-
11	-	-	-0.5236	-
12	-	-	-0.6545	-
13	0.7854	-	-	-
14	1.0354	-	-	-
15	1.2854	-	-	-
16	1.5354	-	-	-
17	1.7854	-	-	-
18	2.0354	-	-	-
19	2.2854	-	-	-
20	2.5354	-	-	-

TABLE I.- Cont'd

21	-	-	0.655	-	
23	-	-	0.855	-	
24	-	0.0	0.955	-	
25	-	-	1.33	-	
26	-	-	1.705	-	
27	-	-	2.08	-	
28	-	-	2.455	-	
29	-	0.25	-	-	
30	-	0.5	-	-	
31	-	0.75	-	-	
32	-	1.0	-	-	
34	-	1.5	-	-	
35	-	1.75	-	-	
36	-	2.0	-	-	
44	-	-	-	315.	WINDOW 1
45	-	-	-	228.	WINDOW 1
46	-	-	-	135.	WINDOW 1
47	-	-	-	45.	WINDOW 1
48	-	-	-	0.0	WINDOW 1
49	-	-	-	330.	WINDOW 1
50	-	-	-	270.	WINDOW 1
51	-	-	-	210.	WINDOW 1
52	-	-	-	150.	WINDOW 1
53	-	-	-	90.	WINDOW 1
54	-	-	-	30.	WINDOW 1

TABLE I.- Cont'd

55	-	-	-	315.	WINDOW 2 — WINDOW RING
56	-	-	-	225.	
57	-	-	-	135.	
58	-	-	-	45.	
59	-	-	-	0.0	
60	-	-	-	60.	WINDOW 2 — OUTER RING
61	-	-	-	0.0	
62	-	-	-	300.	
63	-	-	-	240.	
64	-	-	-	180.	

CONFIGURATION II

Thermocouple	α (°)	
1	0.0	WINDOW 1 — WINDOW RING
2	26.5	
3	115.	
4	212.	
5	286.	
6	337.	WINDOW 1 — MIDDLE RING
7	49.	
8	115.	
9	192.5	
10	235.5	
11	286.	

TABLE I.- Cont'd

12	0.0	OUTER RING	WINDOW 1
13	72.5		
14	151.		
15	212.		
16	259.		
17	310.		
18	0.0	WINDOW RING	WINDOW 2
19	0.0		
20	80.5		
21	180.		
22	250		
23	310.5	MIDDLE RING	
24	22.		
25	80.		
26	152.		
27	201.		
28	250.		
29	336.5	OUTER RING	
30	42.5		
31	109.		
32	180.		
33	223.5		
34	276.5		

TABLE II.- TEST MATRIX

P_t (pa)	Re_∞/meter	$\dot{m}_c/\dot{m}_\infty$ Range	Configuration Tested	Oil Flow
2.41×10^6	1.64×10^6	0.0 → 2.92	I & II	(1) Zero-Mass Injection, I & II (2) $\dot{m}_c/\dot{m}_\infty$ = 0.487. 0.974, 1.64, I
5.16×10^6	3.12×10^6	0.0 → 1.36	I & II	(1) Zero-Mass Injection, I & II
6.88×10^6	4.27×10^6	0.0 → 0.512	I	(1) Zero-Mass Injection, I
8.6×10^6	5.25×10^6	0.0 → 0.818	I	(1) Zero-Mass Injection, I
9.6×10^6	5.9×10^6	0.0 → 0.365	I & II	———
12.0×10^6	7.22×10^6	0.0 → 0.585	I	(1) Zero-Mass Injection, I

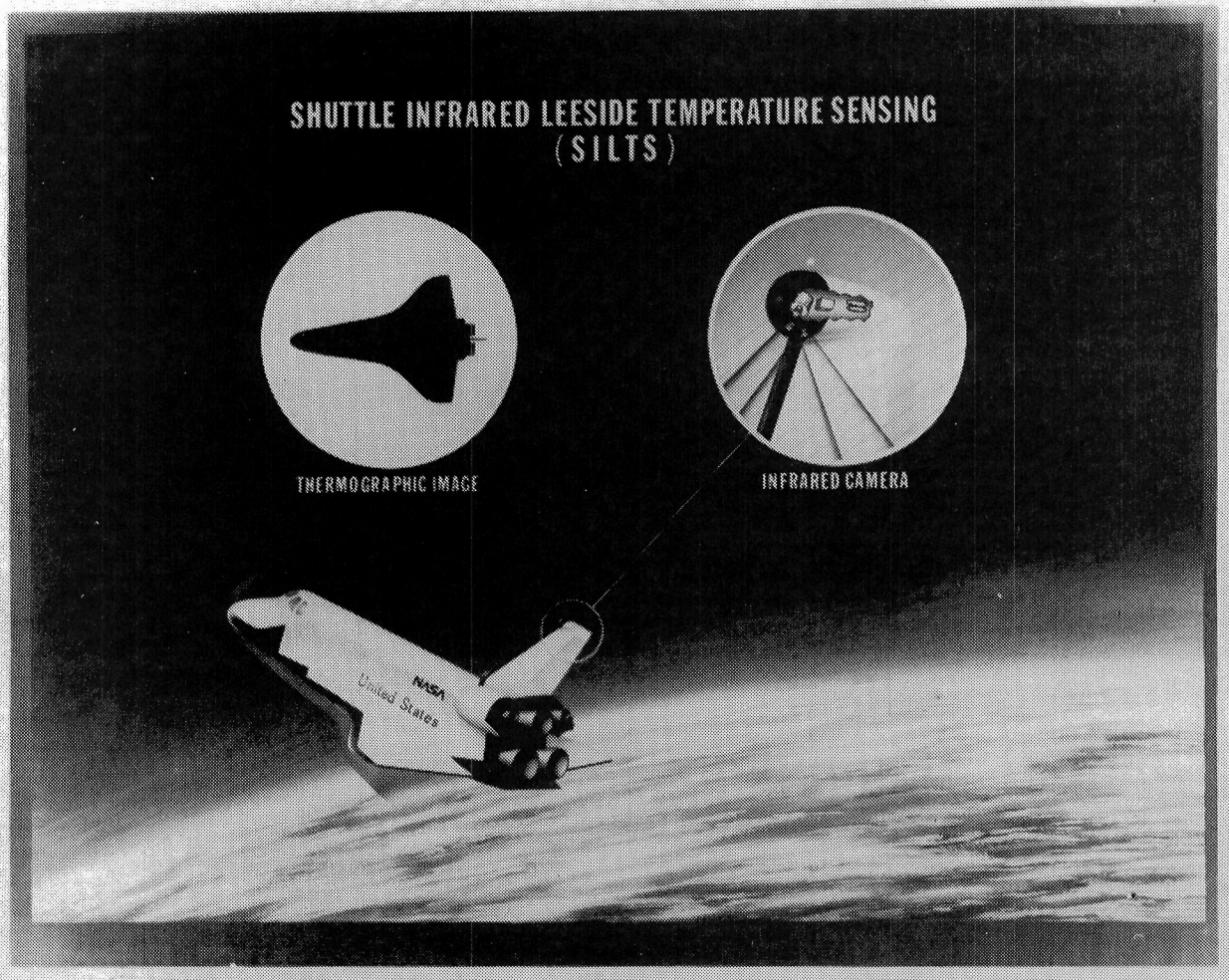

Figure 1.- Shuttle Infrared Leeside Temperature Sensing Experiment.

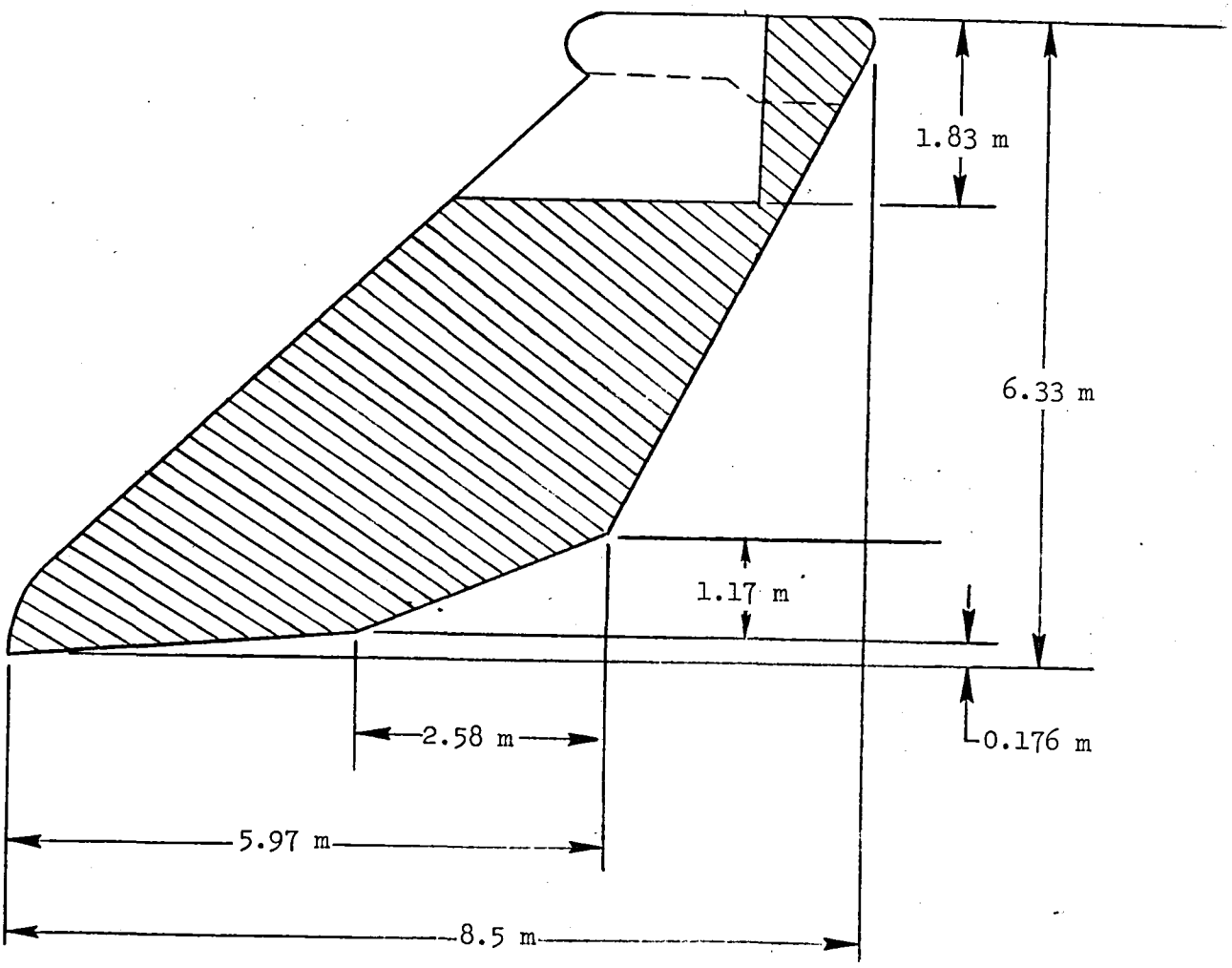

Figure 2.- Portion of vertical tail represented by wind-tunnel model.
(Dimensions are for full-scale orbiter.)

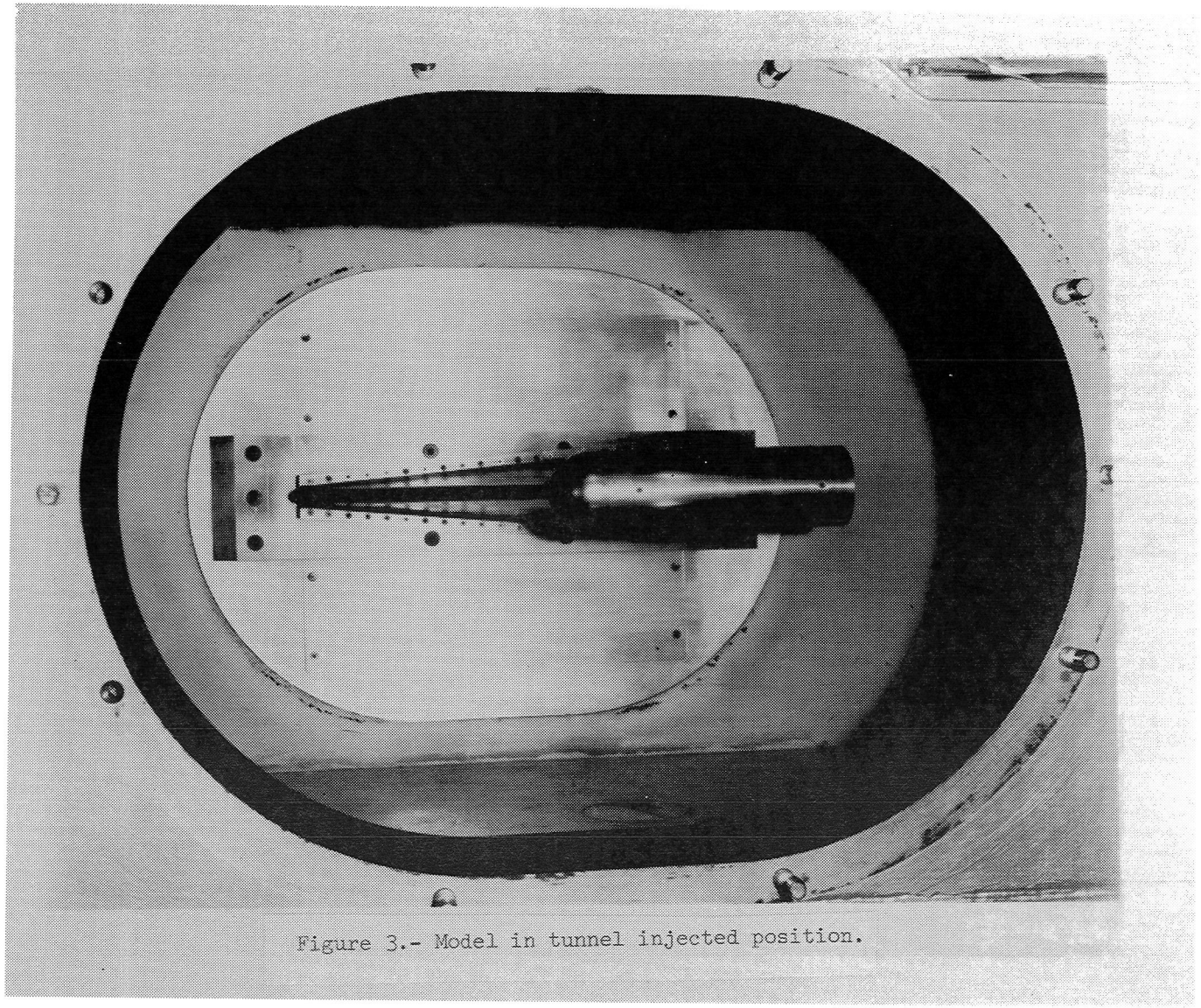

Figure 3.- Model in tunnel injected position.

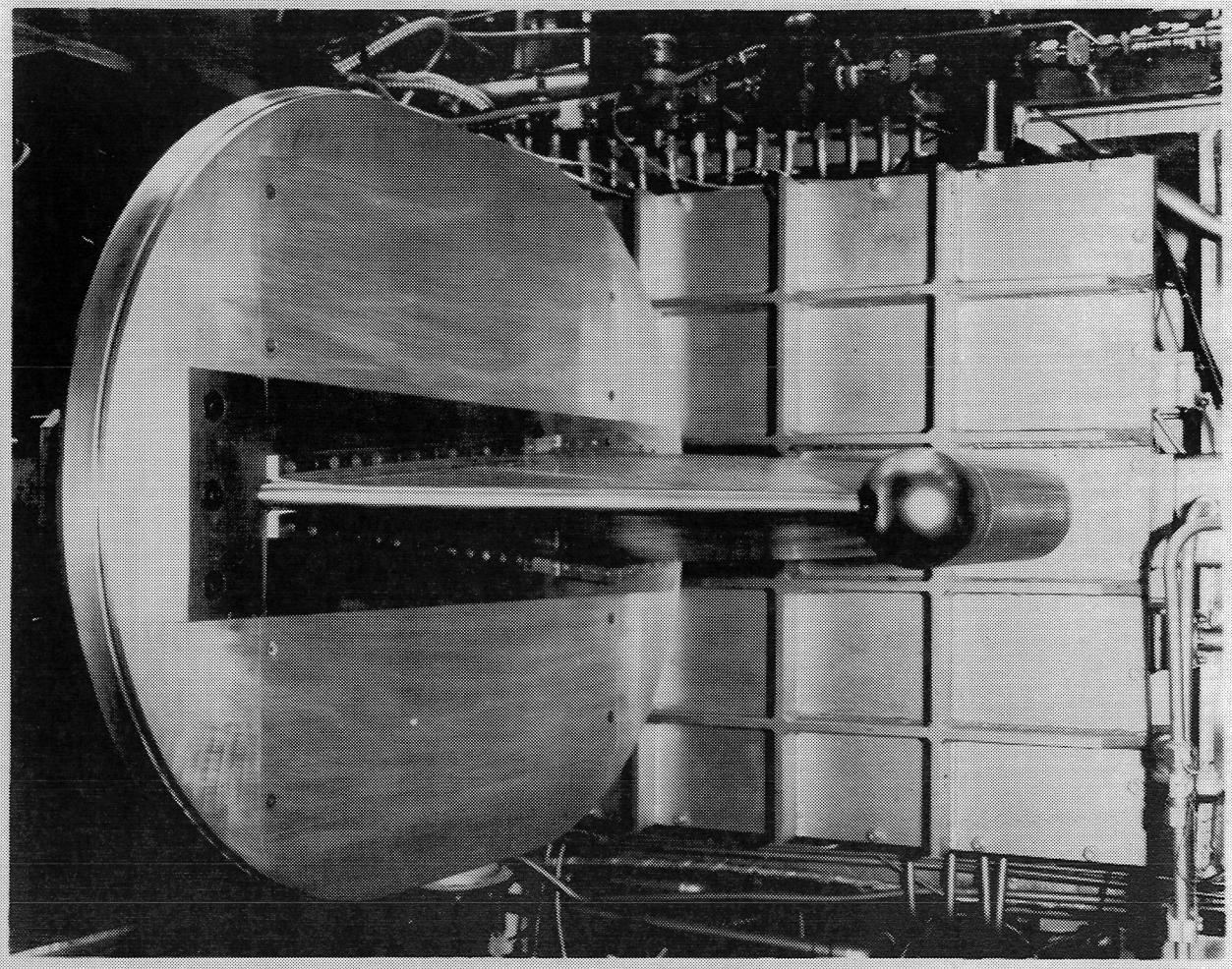

Figure 4.- Model in access position.

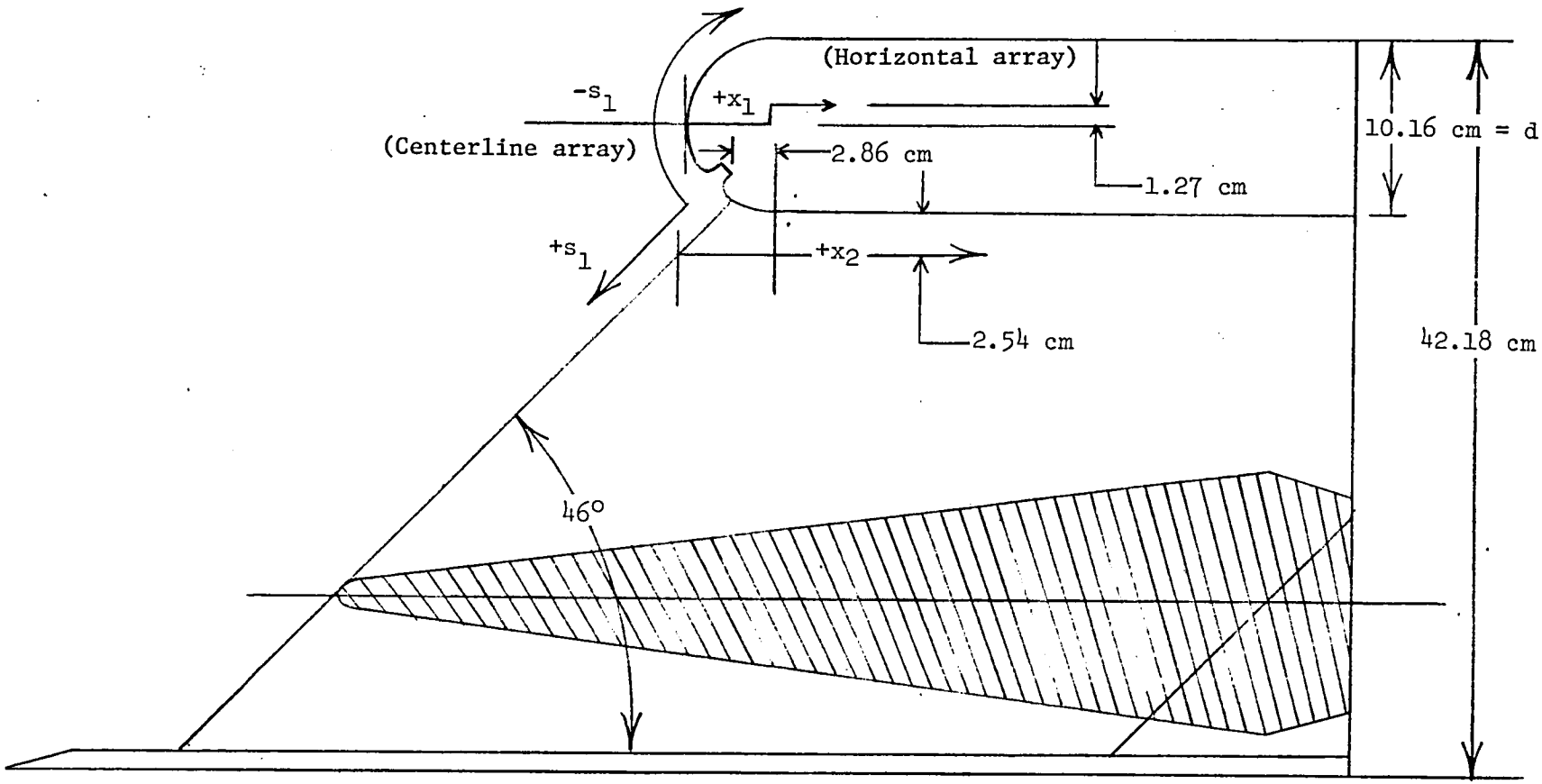

Figure 5.- General model dimensions and thermocouple arrays, Configuration I.
(Side view of model)

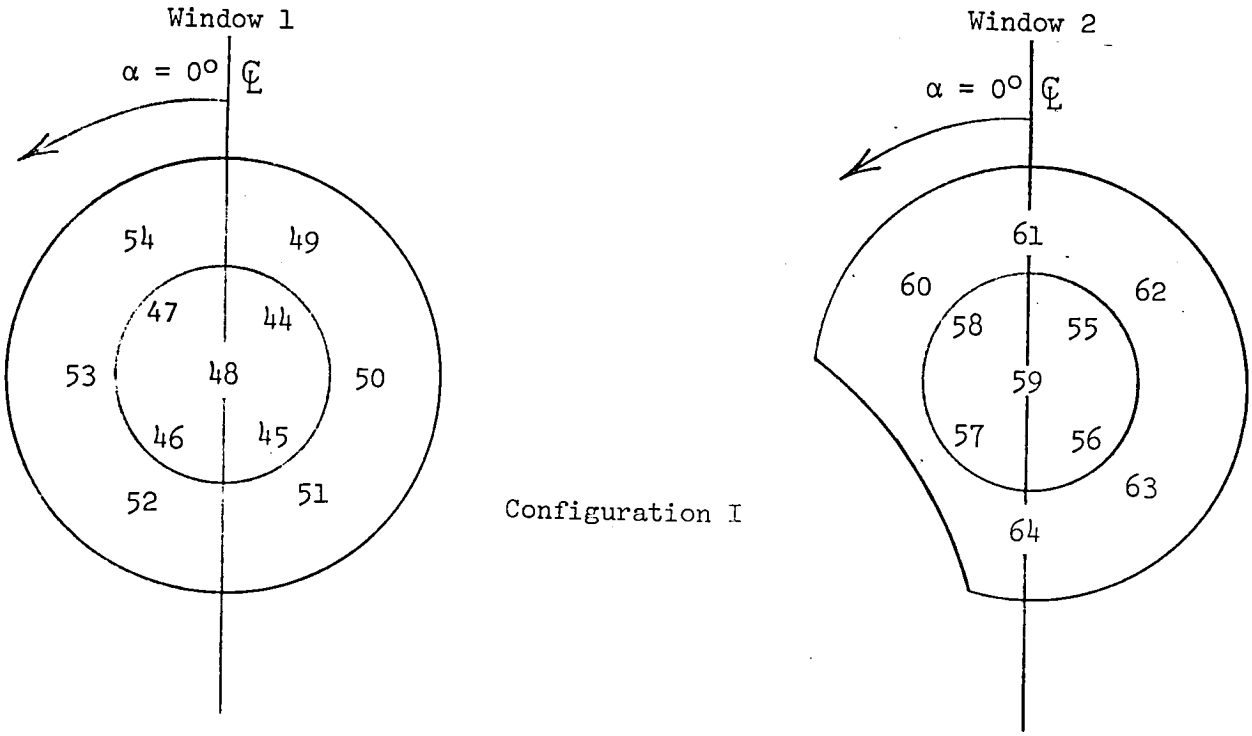

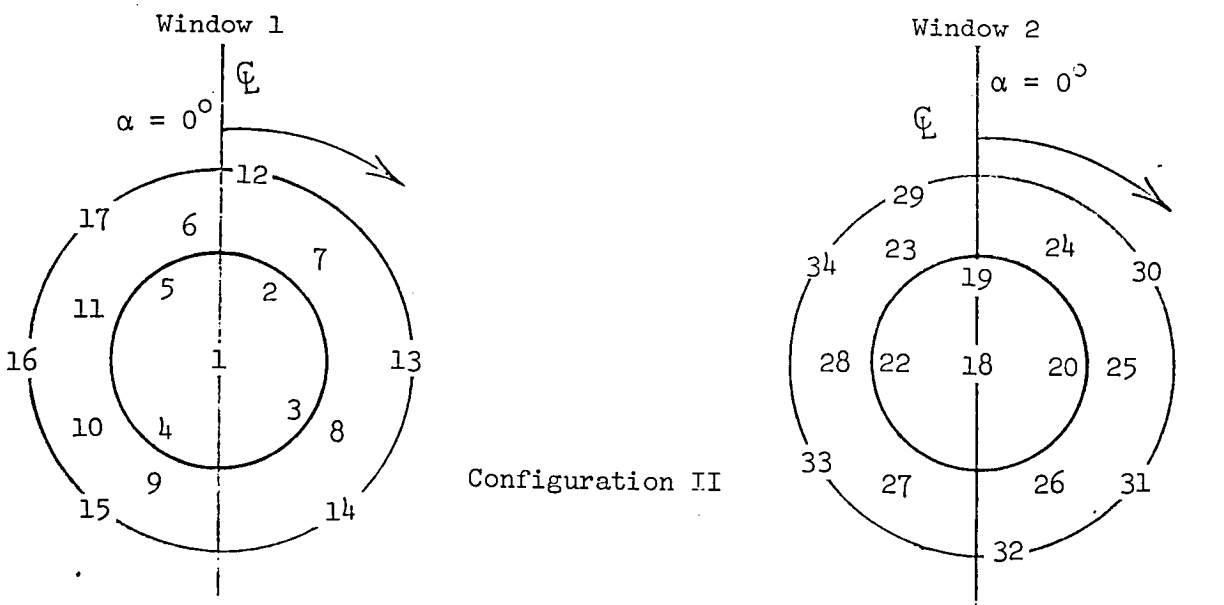

Figure 6.- Thermocouple locations (windows).

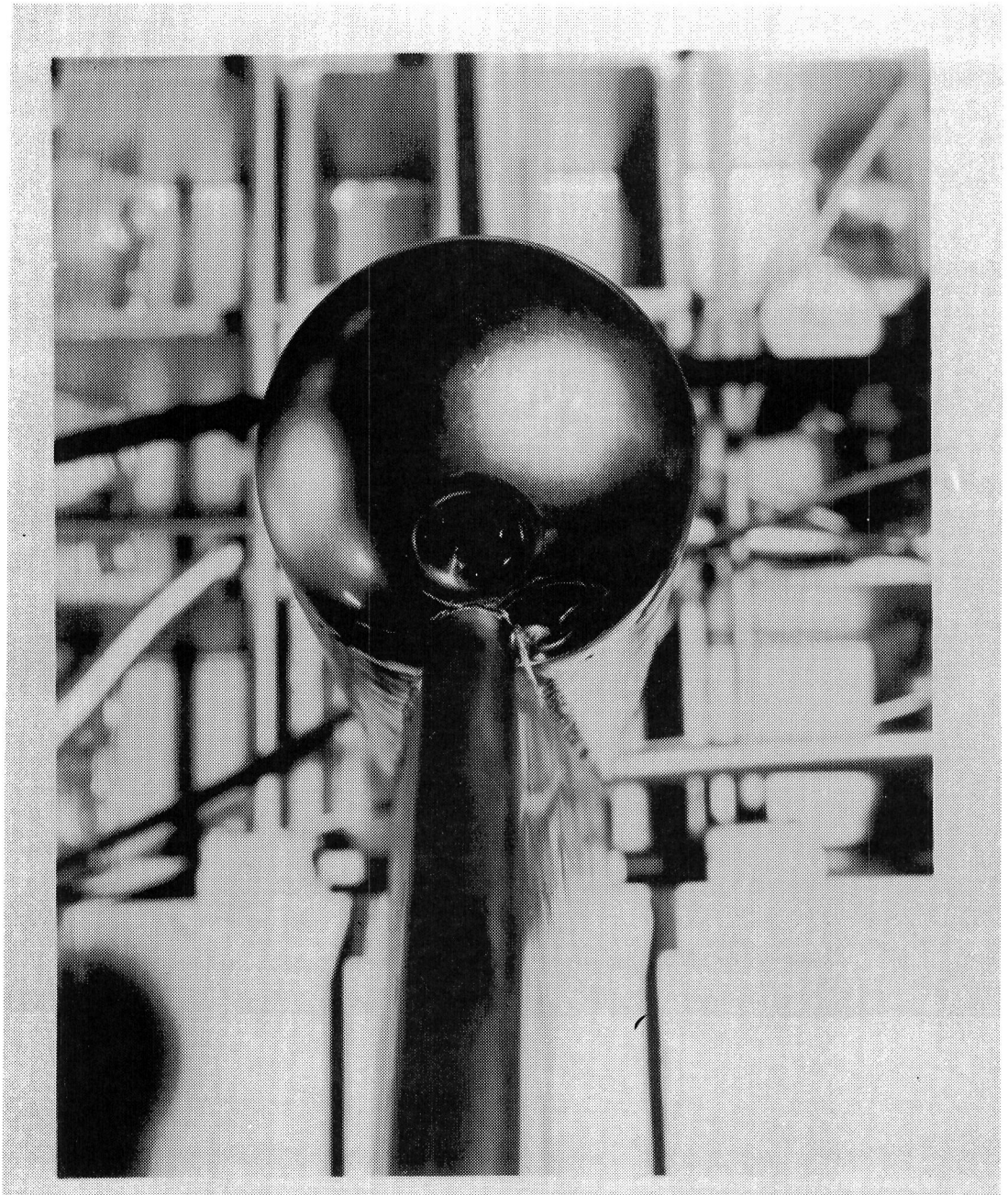

Figure 7.- Closeup of hemisphere, Configuration I.

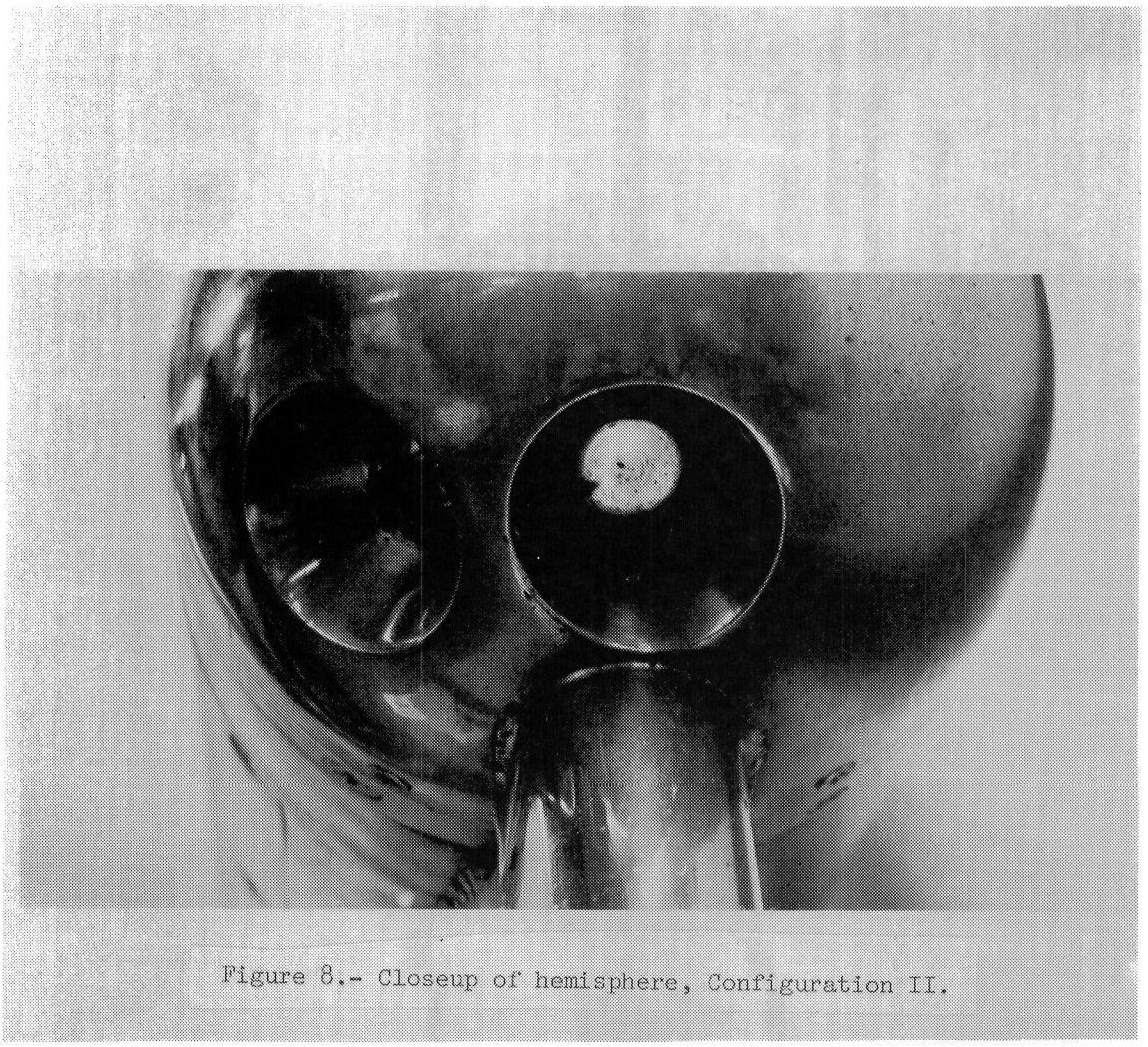

Figure 8.- Closeup of hemisphere, Configuration II.

(1) 4 Coolant (0.265-cm diameter) orifices each window

(2) 4 Thermocouples on a 1.11-cm diameter (window ring)

(3) 6 Thermocouples on a 1.8-cm diameter (middle ring)

(4) 6 Thermocouples on 2.54-cm diameter (outer ring)

(5) Coolant plenum chamber and thermocouple insulation can

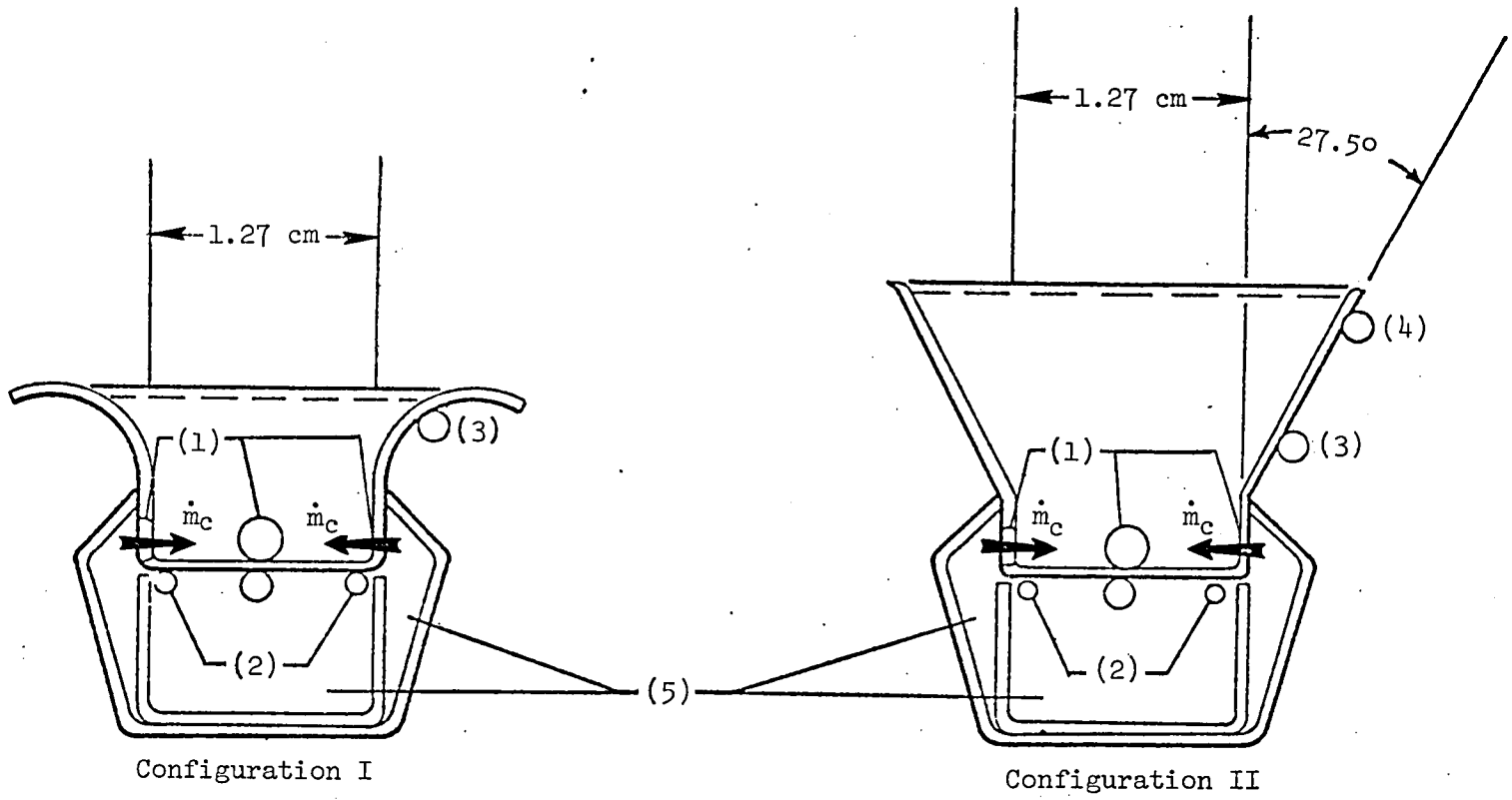

Figure 9.- Window geometries tested.

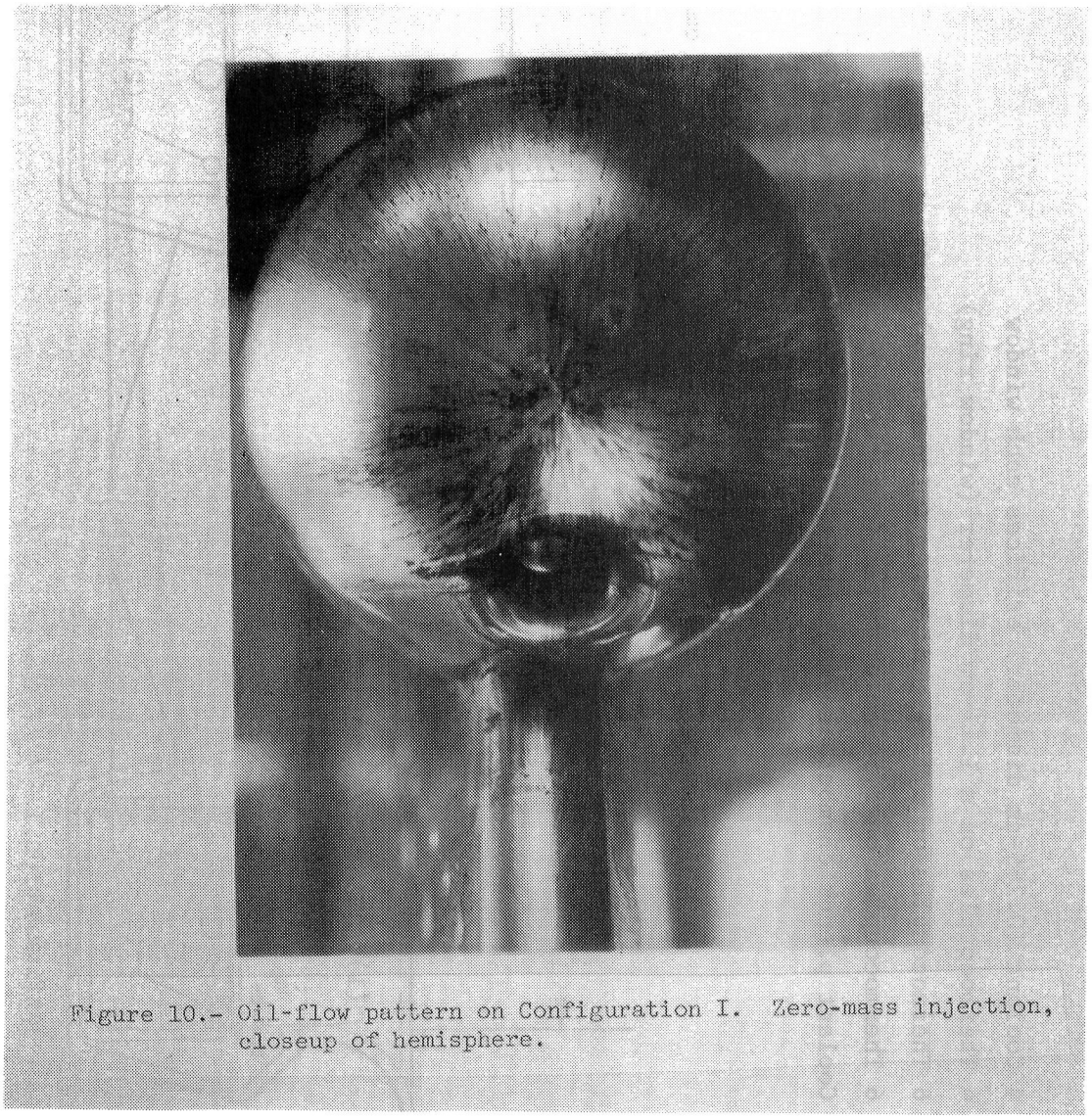

Figure 10.- Oil-flow pattern on Configuration I. Zero-mass injection, closeup of hemisphere.

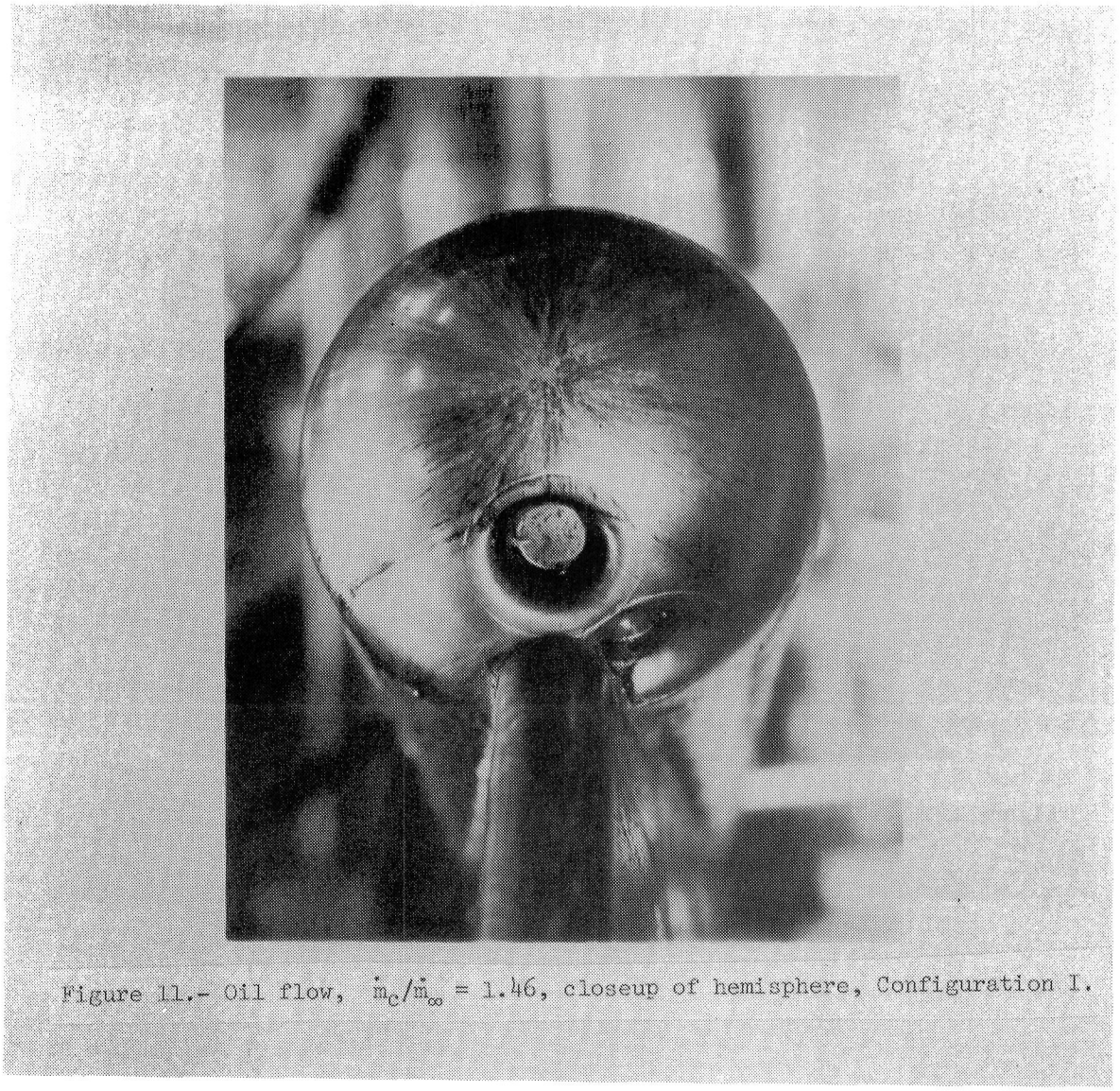

Figure 11.- Oil flow, $\dot{m}_c/\dot{m}_\infty = 1.46$, closeup of hemisphere, Configuration I.

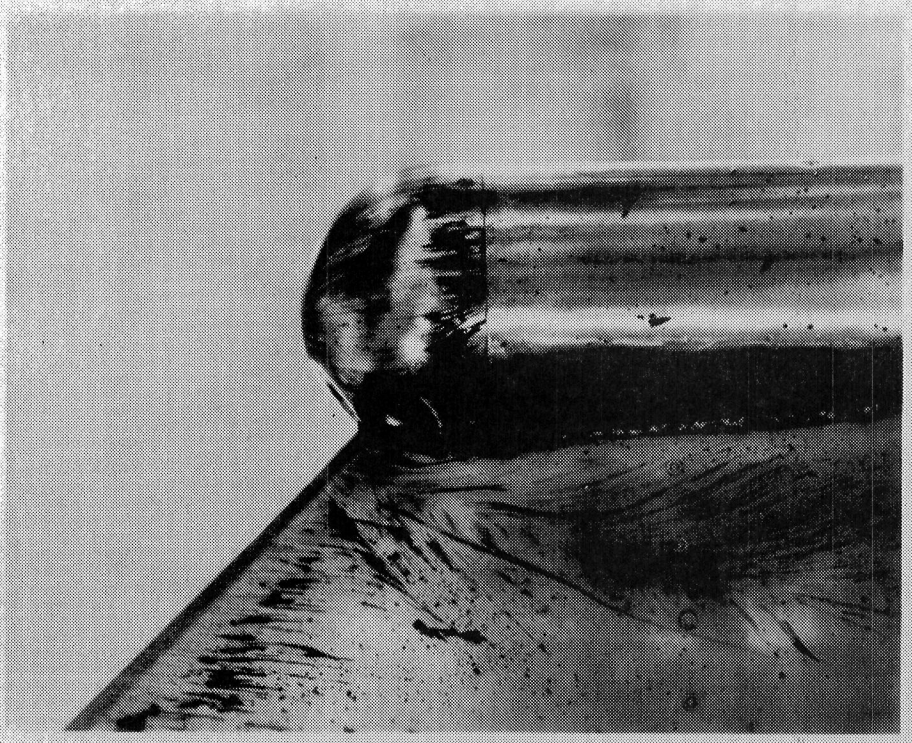

Figure 12.- Oil flow, zero-mass injection, lower view, Configuration I.

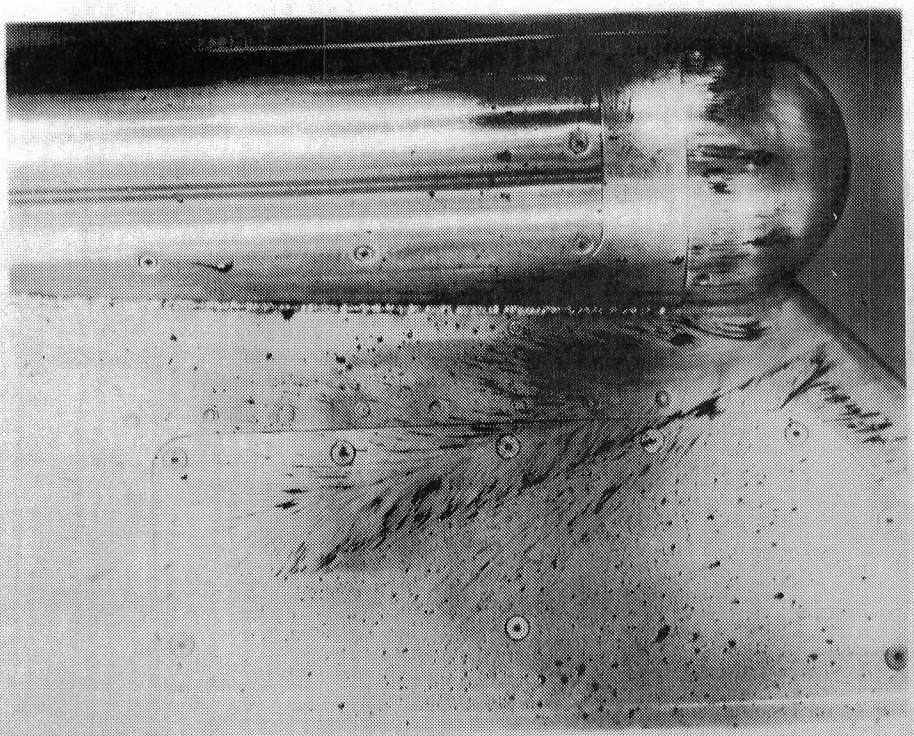

Figure 13.- Oil flow, $\dot{m}_c/\dot{m}_\infty = 1.46$, upper view, Configuration I.

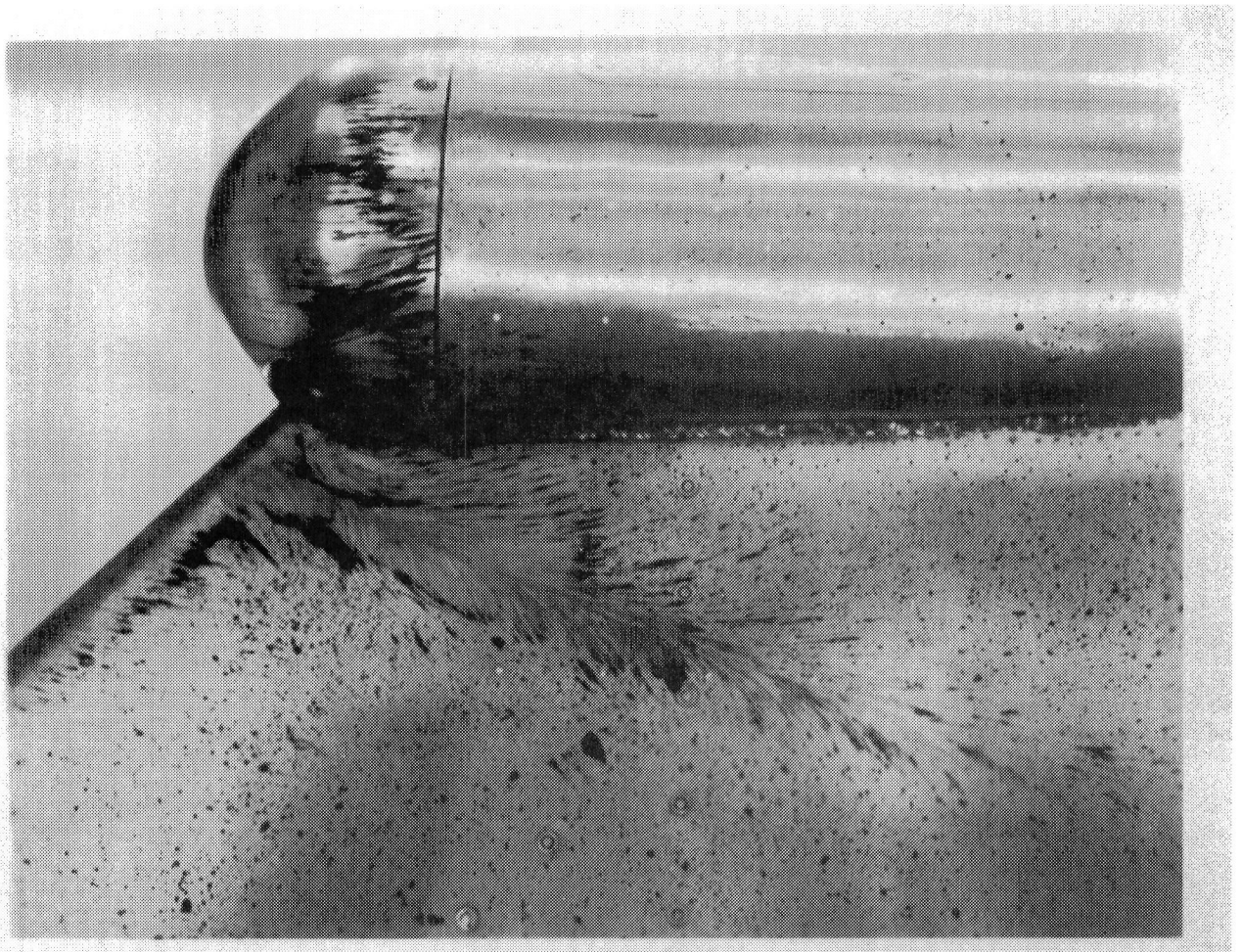

Figure 14.- Oil flow, $\dot{m}_c/\dot{m}_\infty = 1.46$, lower view, Configuration I.

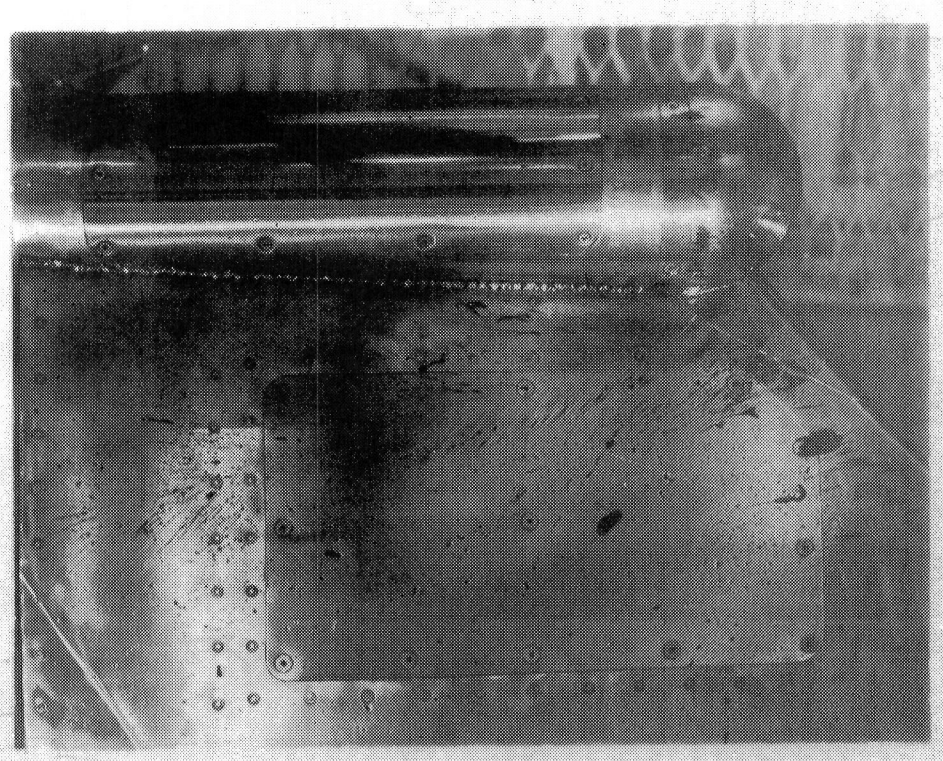

Figure 15.- Oil flow, zero-mass injection, upper view, Configuration II.

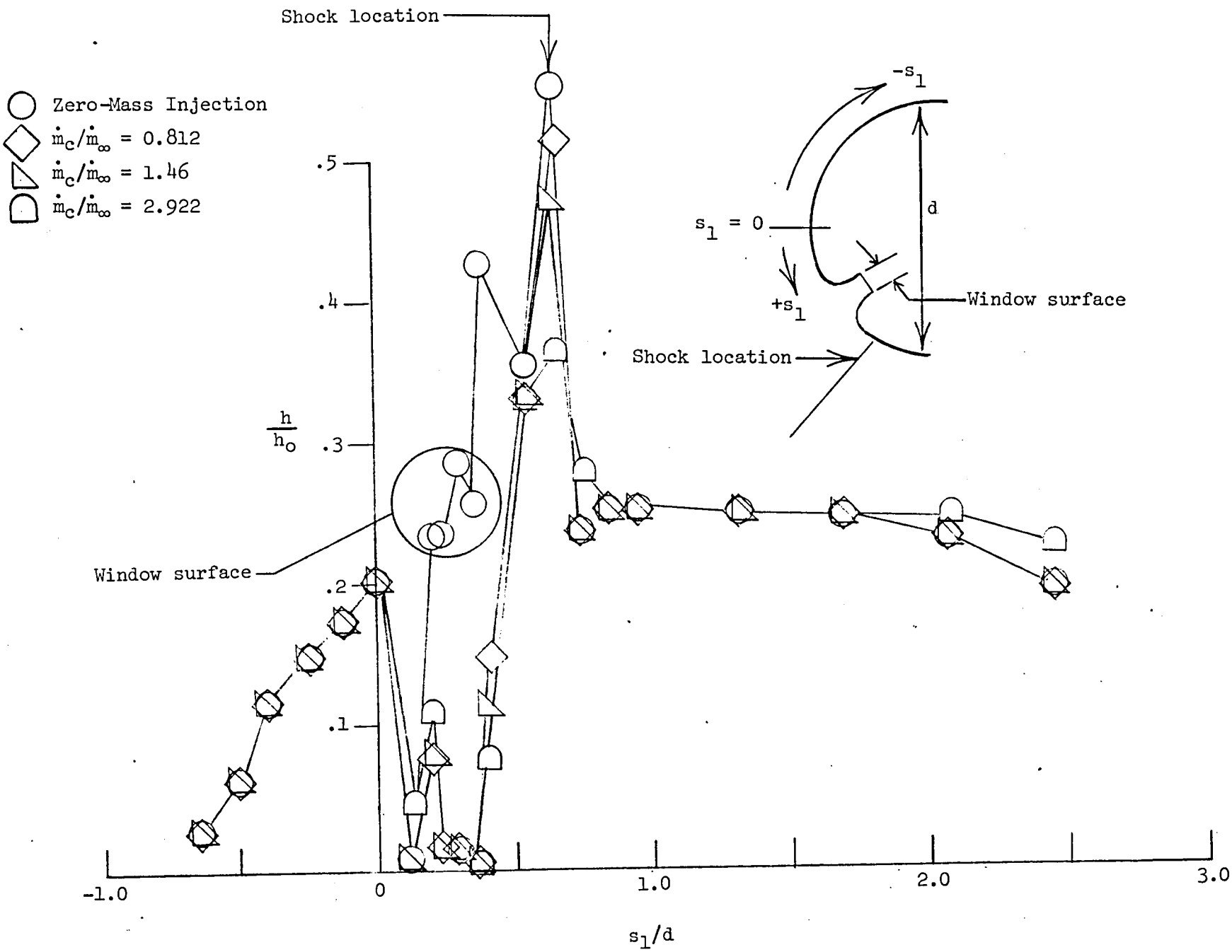

Figure 16.- Centerline heat transfer, Configuration I.

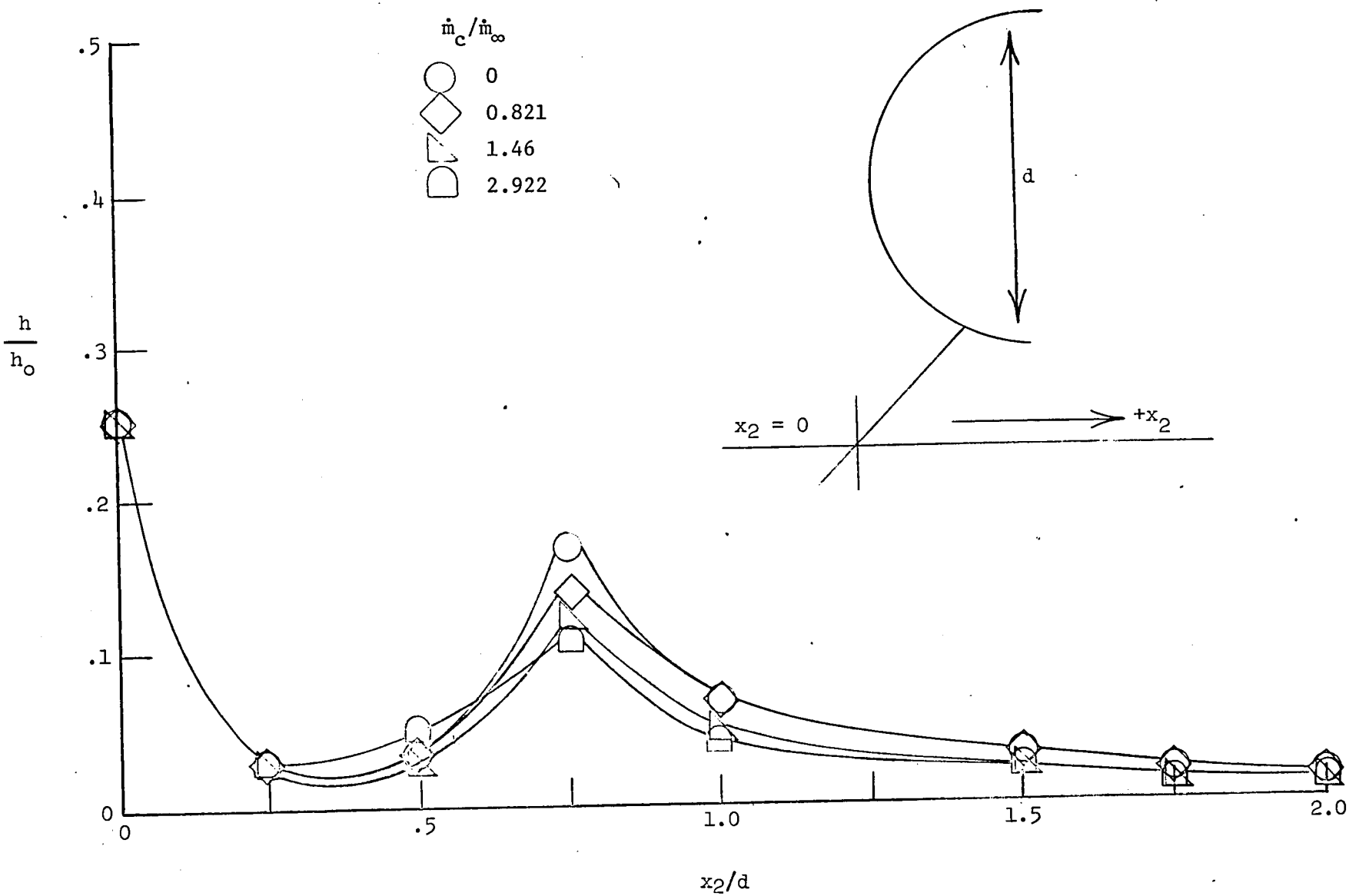

Figure 17.- Fin-surface heat transfer, Configuration I.

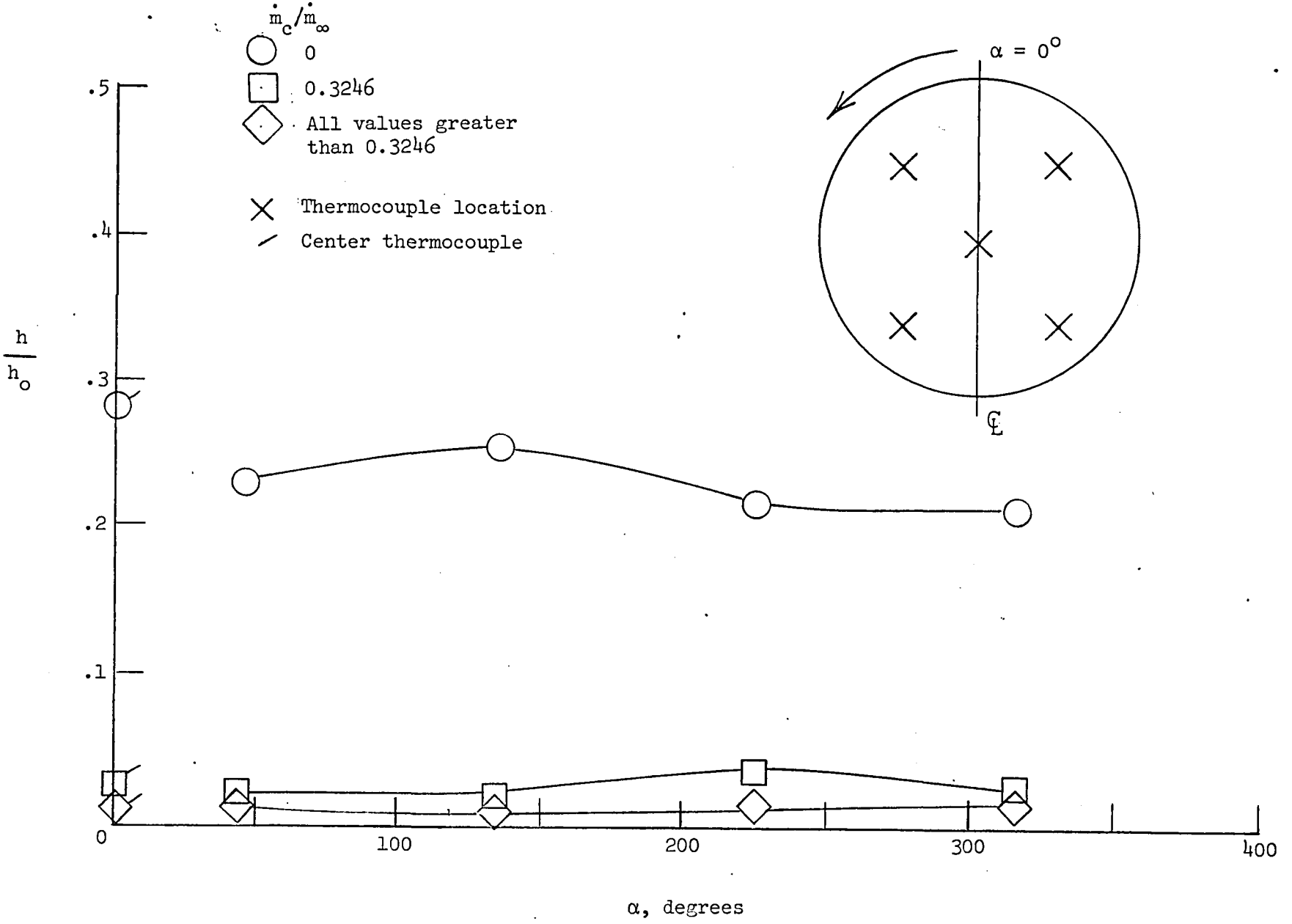

Figure 18.- Heat transfer, window 1, window ring, Configuration I.

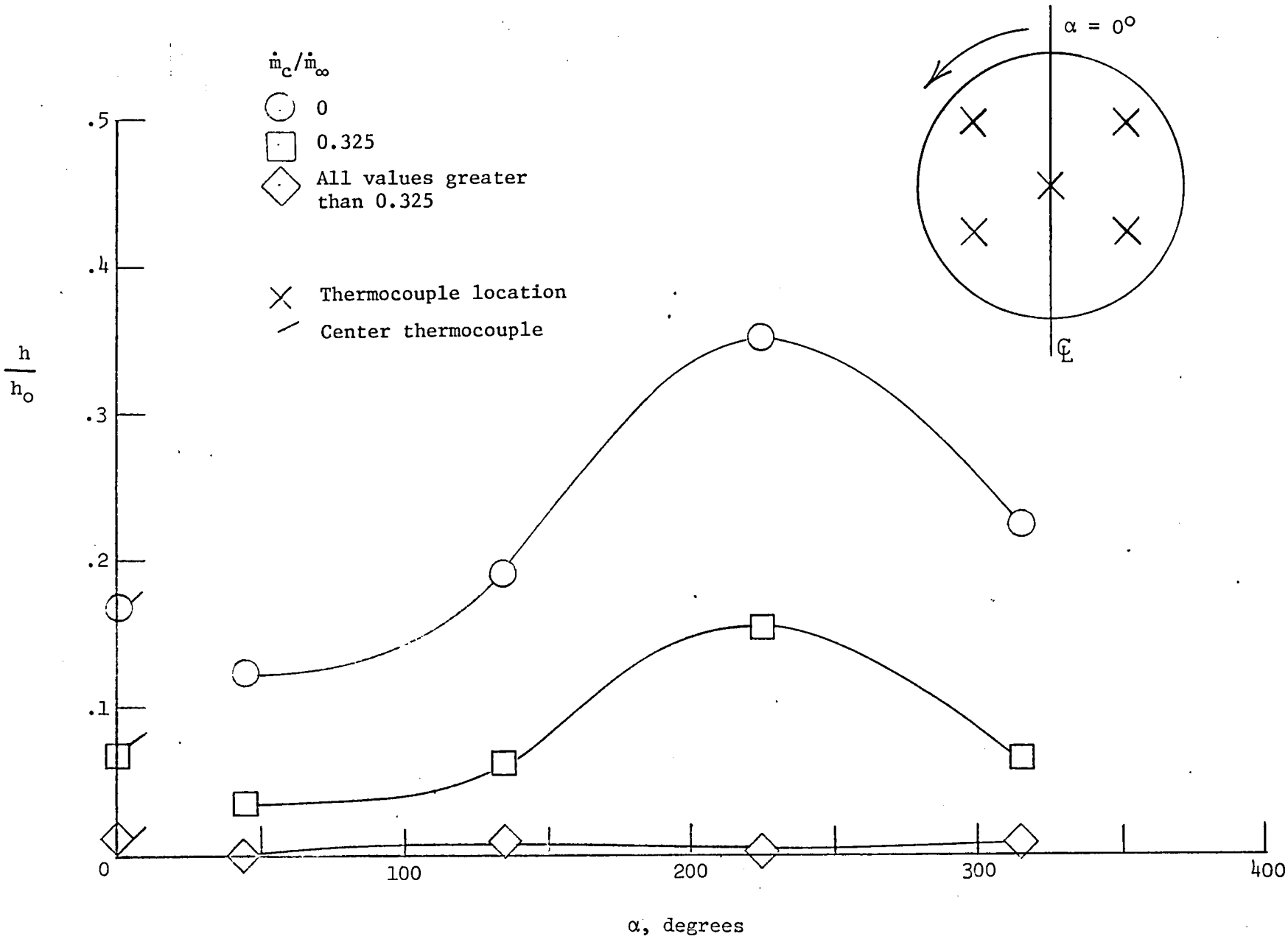

Figure 19.- Heat transfer, window 2, window ring, Configuration I.

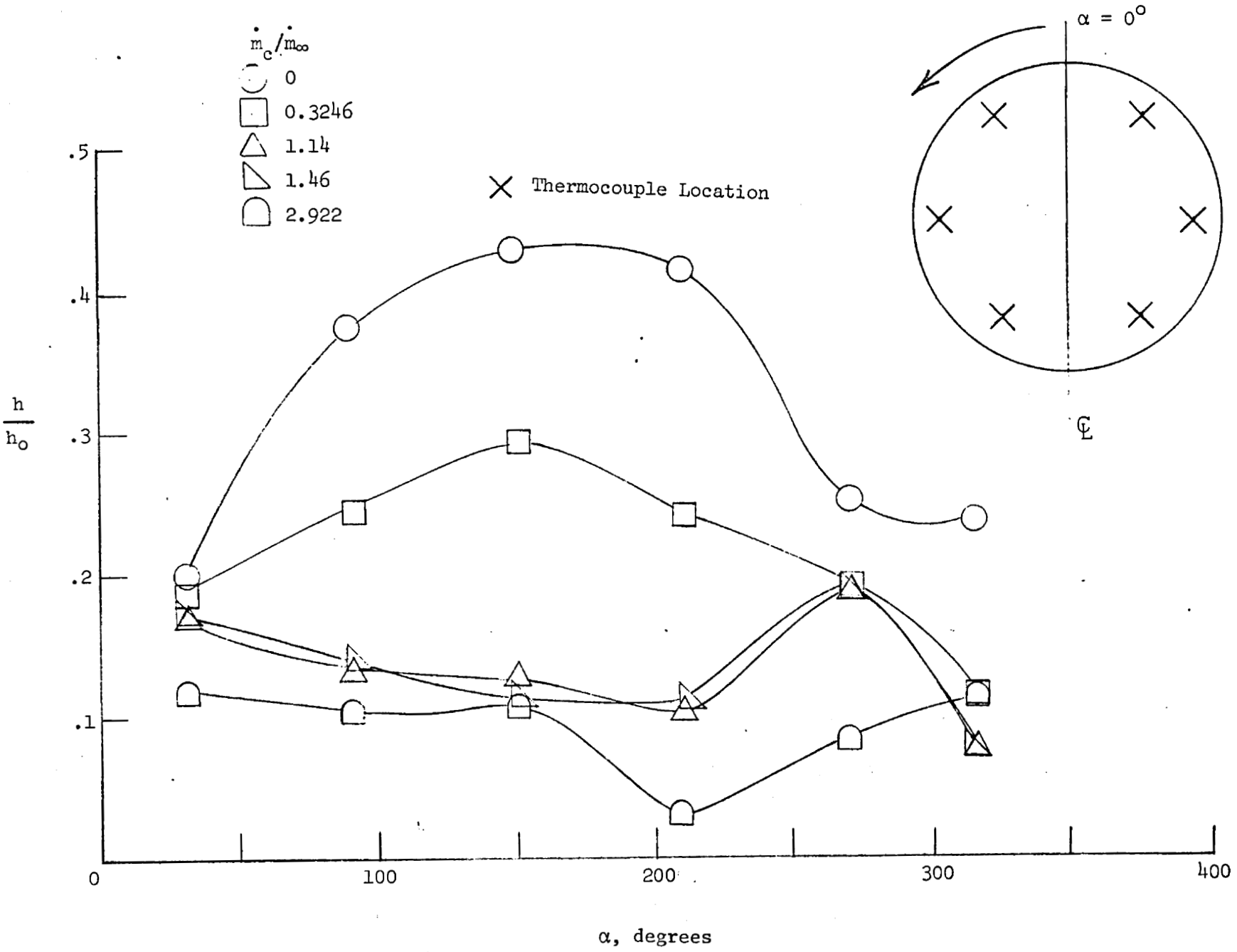

Figure 20.- Heat transfer, window 1, outer ring, Configuration I.

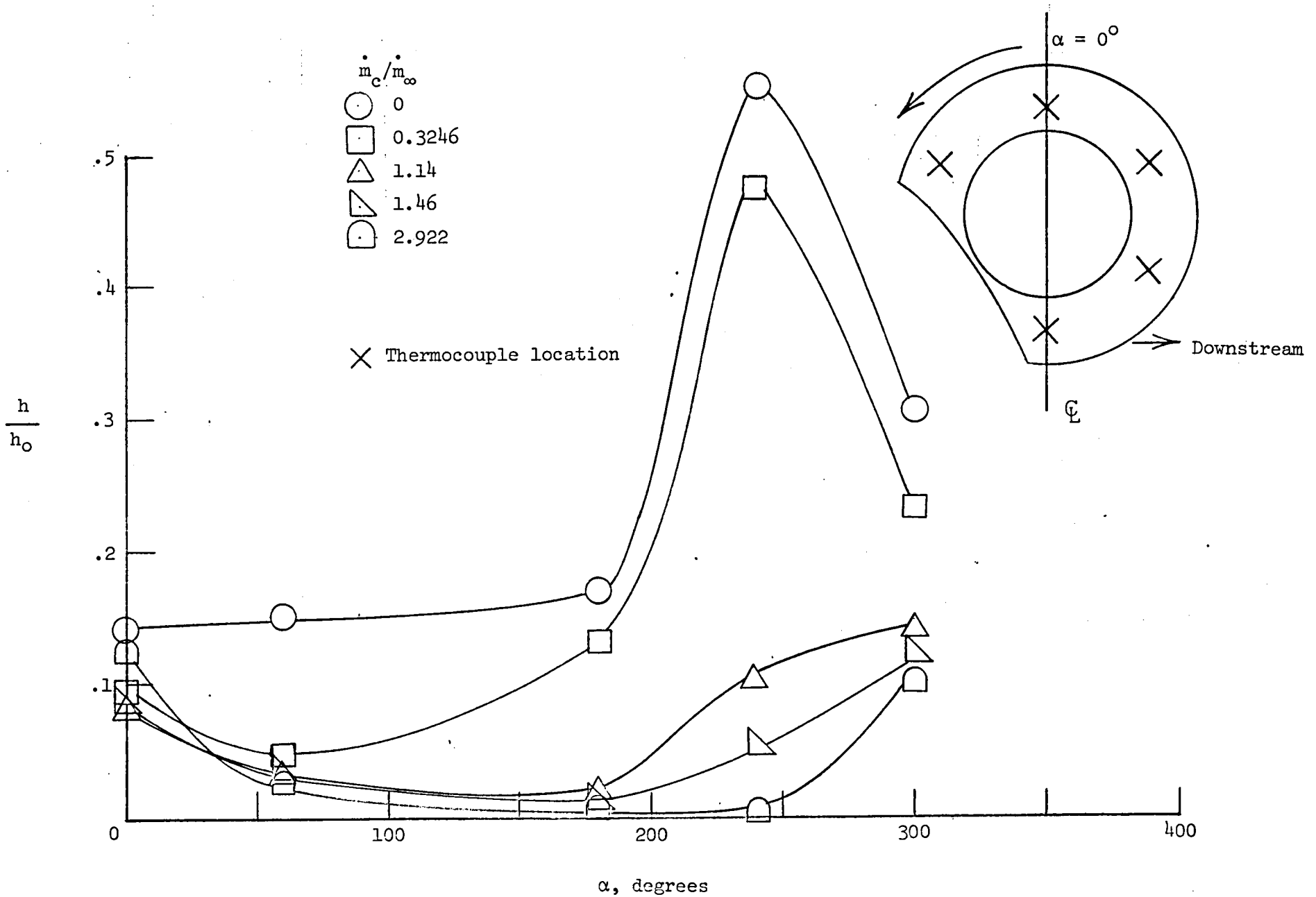

Figure 21.- Heat transfer, window 2, outer ring, Configuration II.

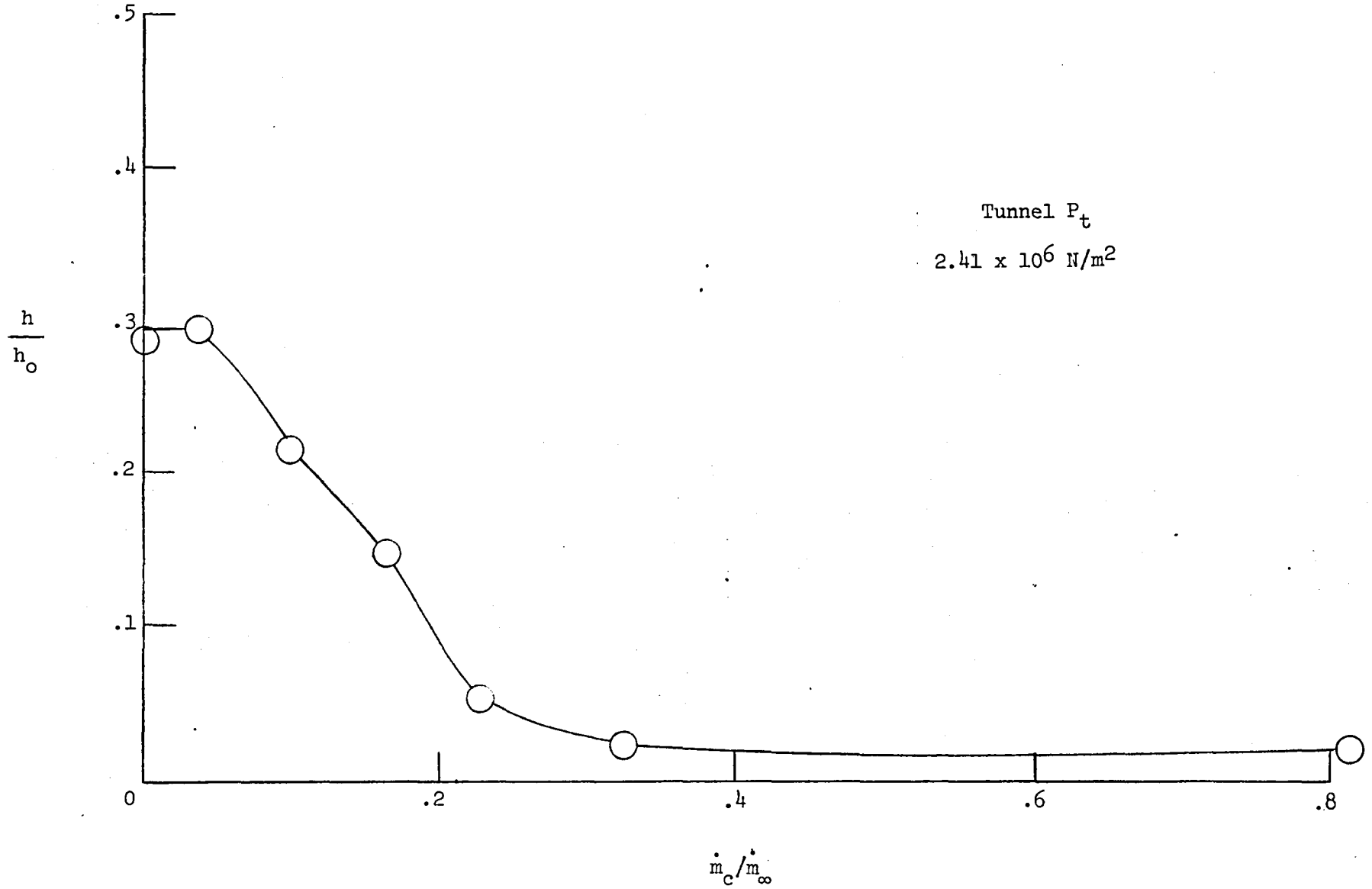

Figure 22.- Heat transfer, thermocouple 48 - center, window 1, Configuration I.

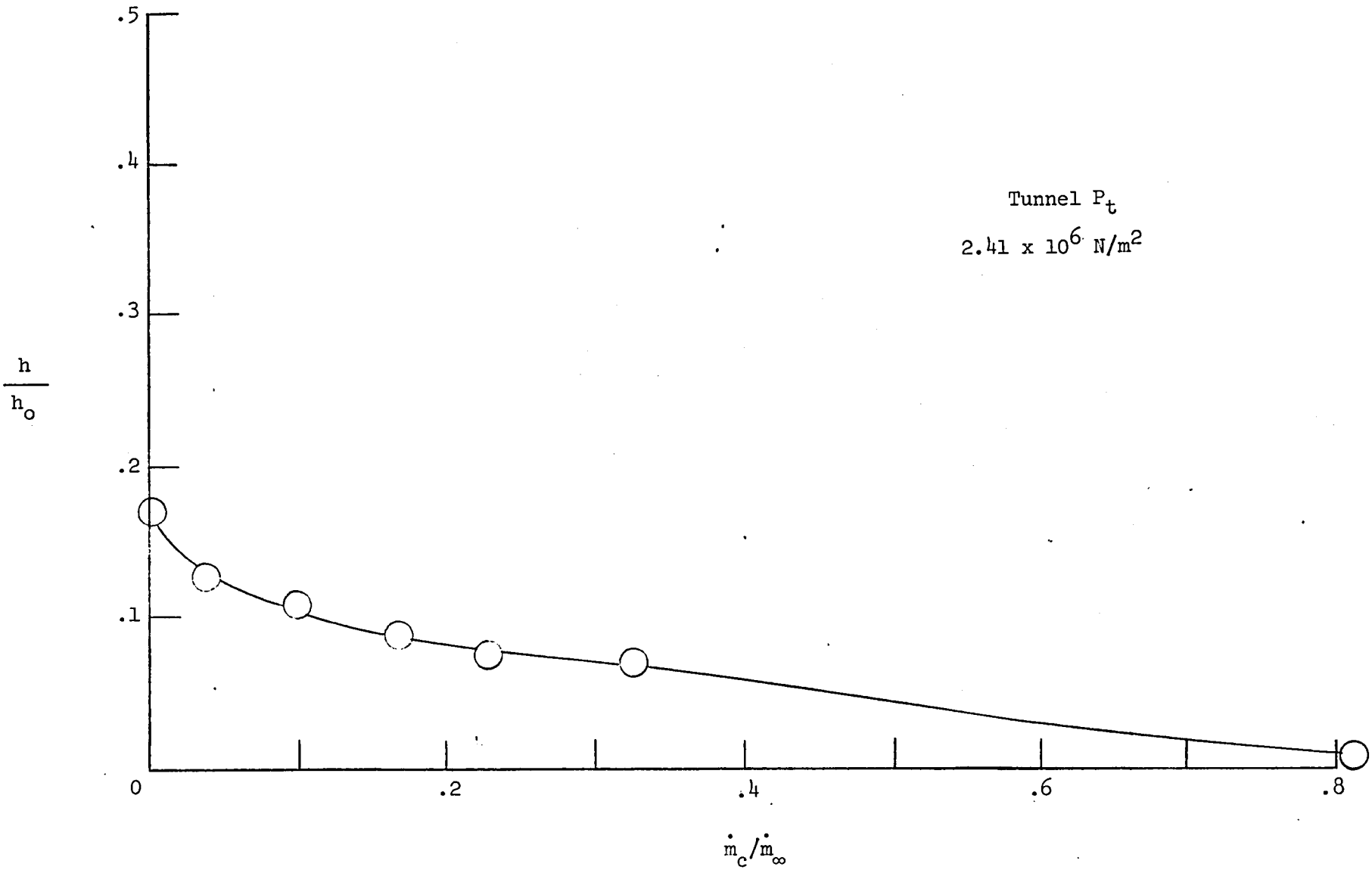

Figure 23.- Heat transfer, thermocouple 59 - center, window 2, Configuration I.

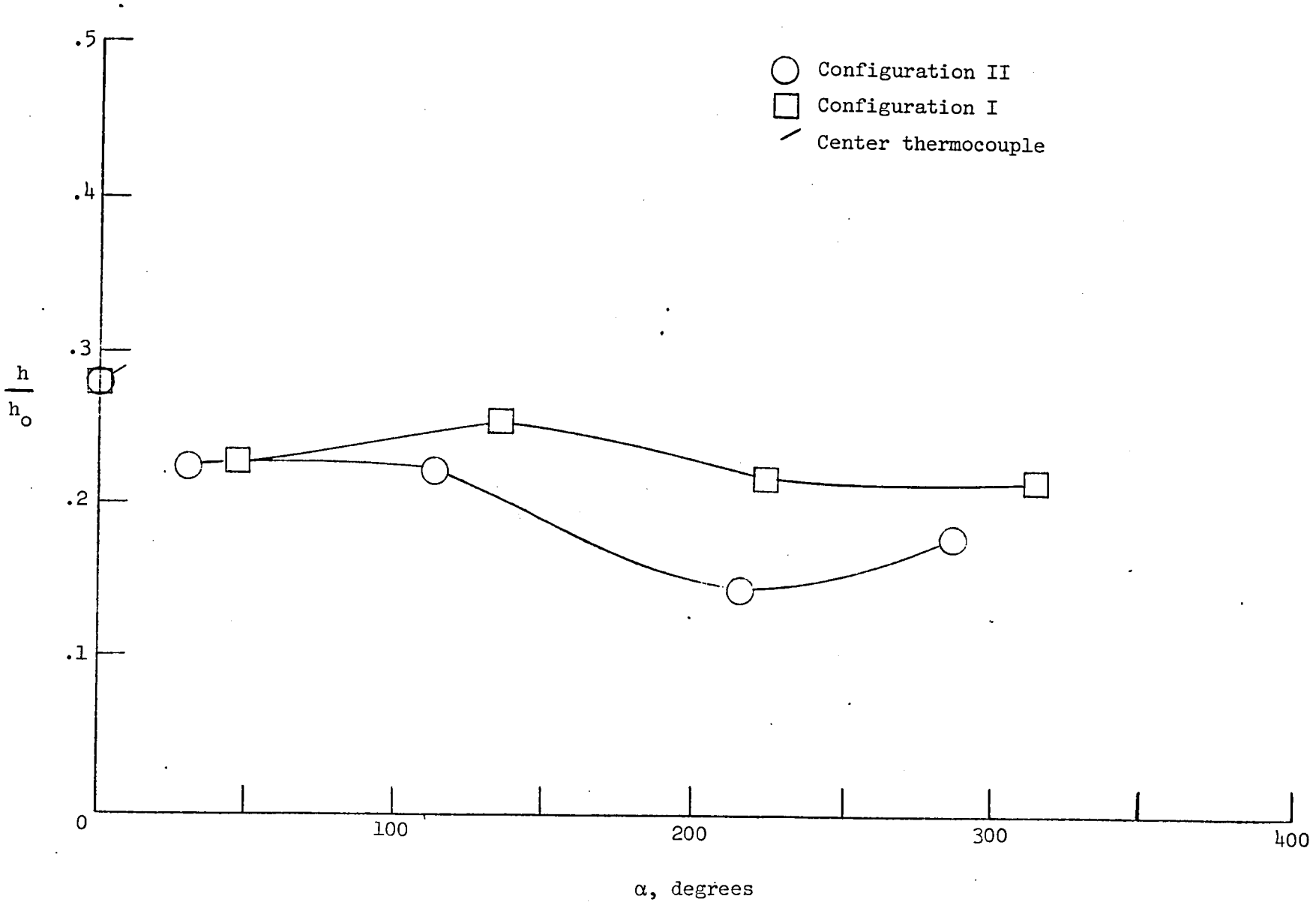

Figure 24.- Heat transfer, window 1, window ring, zero-mass injection.

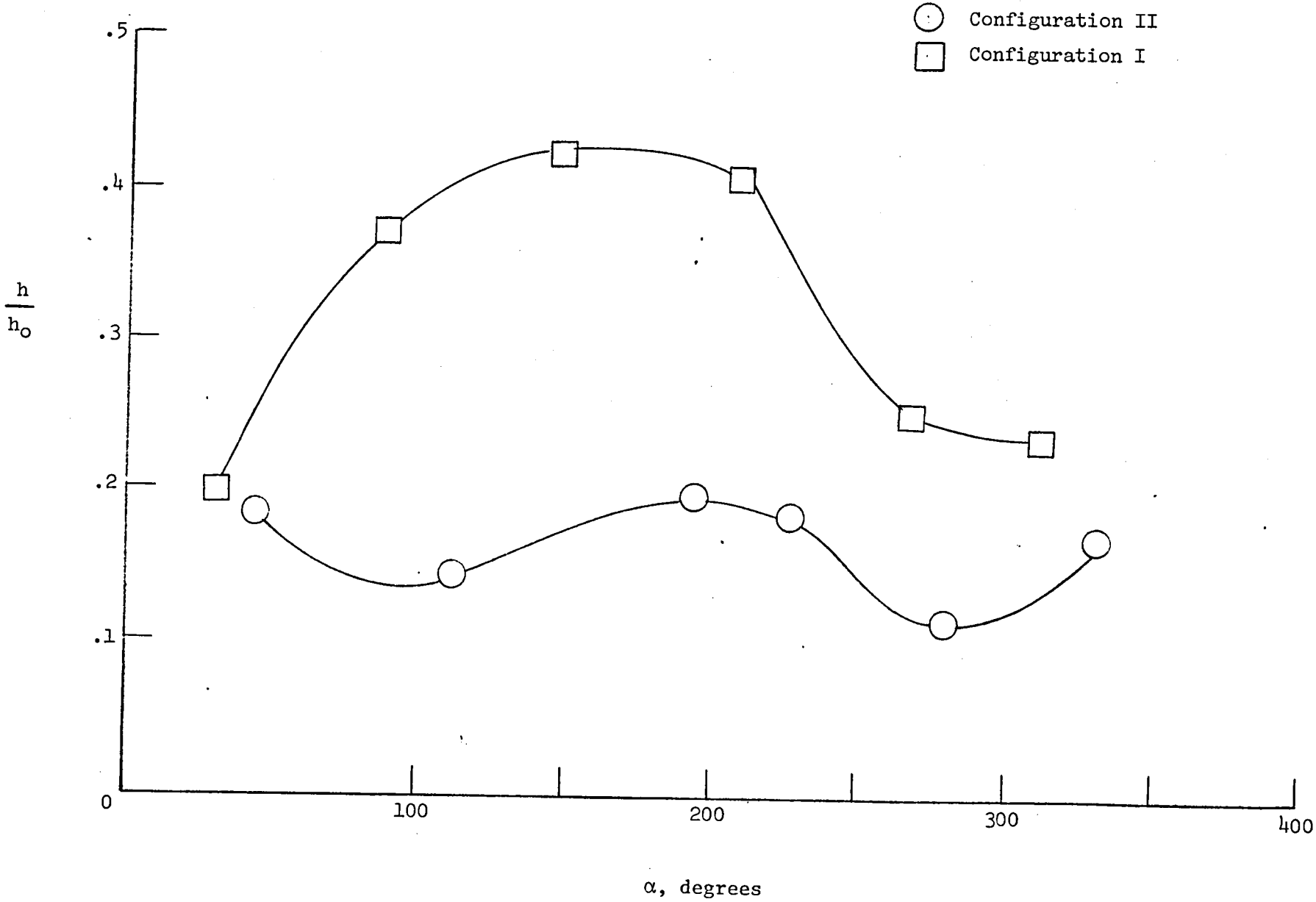

Figure 25.- Heat transfer, window 1, middle ring, zero-mass injection.

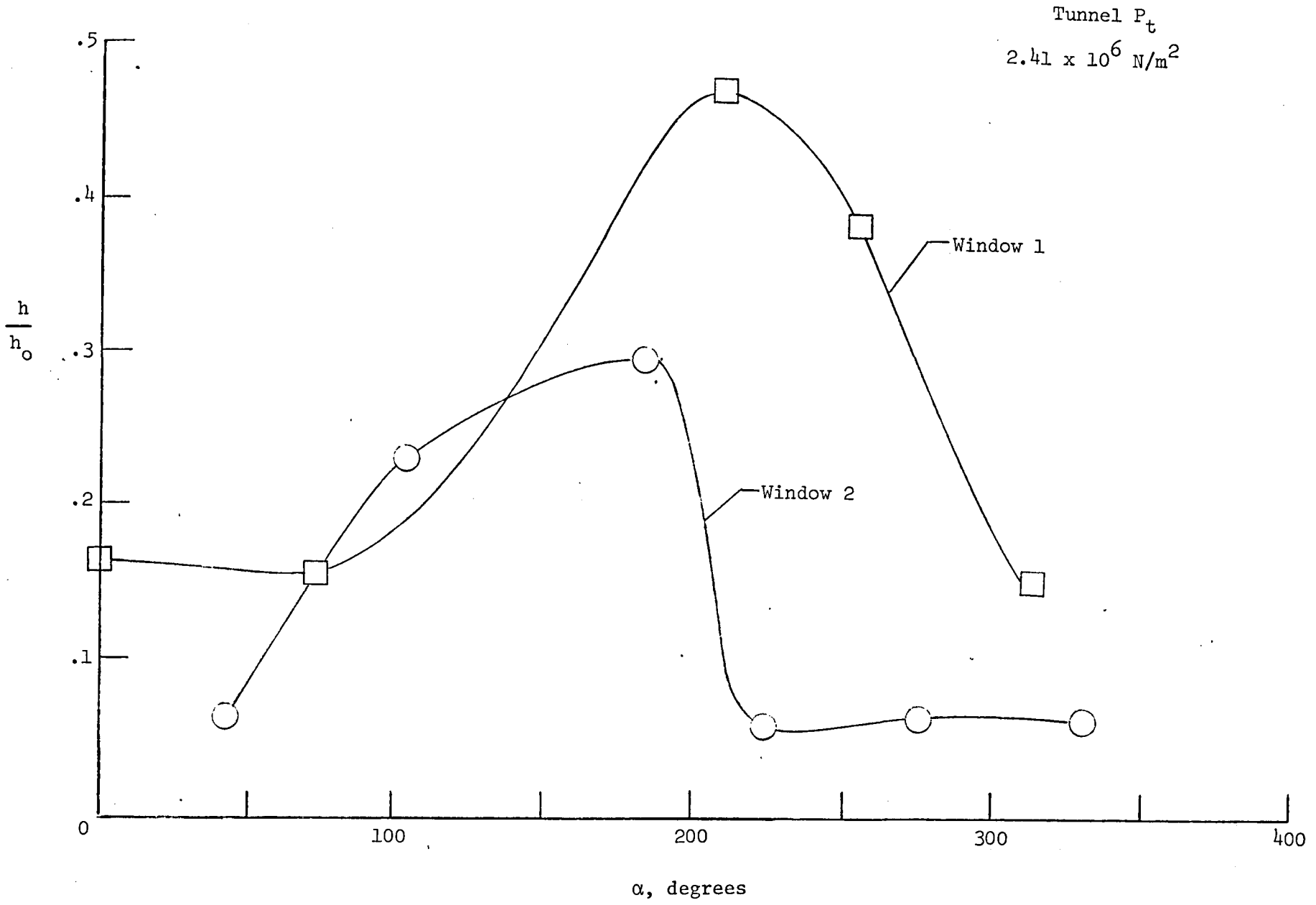

Figure 26.- Heat transfer, windows 1 and 2, outer ring (Configuration II), zero-mass injection.

1. Report No.	2. Government Accession No.	3. Recipient's Catalog No.
NASA TM-80170		

4. Title and Subtitle	5. Report Date
An Experimental Investigation to Determine the Effect of Window Cooling by Mass Injection for the Shuttle Infrared Leeside Temperature Sensing (SILTS) Experiment	September 1979
	6. Performing Organization Code
7. Author(s)	8. Performing Organization Report No.
Pamela F. Bradley	
9. Performing Organization Name and Address	10. Work Unit No.
NASA Langley Research Center Hampton, VA 23665	506-51-13-01
	11. Contract or Grant No.
12. Sponsoring Agency Name and Address	13. Type of Report and Period Covered
National Aeronautics and Space Administration Washington, DC 20546	Technical Memorandum
	14. Army Project No.

15. Supplementary Notes

16. Abstract

An experimental investigation was conducted in the Langley Research Center continuous flow hypersonic tunnel to determine the cooling effect of mass injection on the Shuttle Infrared Leeside Temperature Sensing (SILTS) pod window surfaces. Because high window temperatures will affect the infrared radiation received by the SILTS sensor during reentry, mass injection at the base of the window lenses is used as a means of maintaining low window temperatures. A 0.25-scale stainless-steel model of a portion of the orbiter's vertical stabilizer with a SILTS pod was instrumented with thermocouples in order to determine heat-transfer coefficients on and around the simulated windows and window cavities. Test results are presented for a free-stream Reynolds number of 1.64×10^6 per meter at Mach 10.16.

Two window-cavity configurations were tested. Results indicate that deeper window cavities provide more protection for the window surfaces, especially when there is no mass injection. A coolant mass flow, the order of the local free stream ahead of the pod, will reduce heating to the window surfaces by 90 percent.

17. Key Words (Suggested by Author(s))	18. Distribution Statement
Heat transfer Hypersonic wind tunnel testing Shuttle orbiter experiments Film cooling	Unclassified - Unlimited Subject Category 34

19. Security Classif. (of this report)	20. Security Classif. (of this page)	21. No. of Pages	22. Price*
Unclassified	Unclassified	42	$4.50

*For sale by the National Technical Information Service, Springfield, Virginia 22161